2009-01-01

Lipid Metal Organic Networks

Maria Eugenia Martinez
University of Texas at El Paso, mibellajenno@gmail.com

LIPID METAL ORGANIC NETWORKS

MARIA EUGENIA MARTINEZ ORTEGA

Department of Chemistry.

APPROVED:

Juan C. Noveron, Ph.D., Chair

Russell R. Chianelli, Ph.D.

John Mc Clure, Ph.D.

Patricia D. Whiterspoon, Ph.D.
Dean of the Graduate School

Dedication

TO MY MOTHER MARIA LUISA ORTEGA

LIPID METAL ORGANIC NETWORKS

by

MARIA EUGENIA MARTINEZ ORTEGA

THESIS

Presented to the Faculty of the Graduate School of

The University of Texas at El Paso

in Partial Fulfillment

of the Requirements

for the Degree of

MASTER OF SCIENCE

Department of Chemistry

THE UNIVERSITY OF TEXAS AT EL PASO

May 2009

Acknowledgements

This research would not have been possible without the aid and support of countless people. I would like to thank my advisor Dr. Noveron for his invaluable assistance, support and guidance. His suggestions about this research thesis project made more valuable work. Special thanks to Dr. Noveron's laboratory group Alex, Alma, Gaby, Hugo, Luis, Gabriel, Noel, Abdullah and Dr Jamal Khamsi for their help and willing to run experimentation and participate with me in obtaining all required information.

I would like to specially thank Brenda Porta for her help and recommendations during whole thesis investigation process. Thank you Alex Escobar and Dr Claudia A. Rodriguez for all your support to fulfill this big challenge of finish up master's thesis. To my beloved mom that always support my initiative.

Abstract

Metal-organic frameworks (MOFs) first appeared in the literature in 1991[1] and consist of three dimensional structures constructed by linking transition metal ions together through highly directional bonding with organic ligands [2]. MOF materials offer the ability to choose from variety of metal centers that allow the tailoring of optical or magnetic properties, as well as control, to some extent, the size of the coordination sphere [3]. Another advantage is the numerous organic ligands form which suitable pore geometries may be constructed with customized functionality [2] among many applications in other areas such a gas storage [4], chemical separations [5] and selective catalysis [6]. The primary objective of this research was to develop the methodology for the preparation of a new class of MOFs that we call lipid metal organic networks (LMON), which use fatty acid derivatives of biomass in combination with bridging dipyridyl ligands such as 4-4'-Trymethylene dipyridine [7] and transition metal ions to form extended moldable crystalline polymers. The single-crystal X-ray structure of a model LMON is reported in order to provide evidence of the possible molecular structure of LMONs. This thesis presents seven unprecedented LMONs of high molecular weight that exhibit thermoplastic properties at relatively low temperatures.

Table of Contents

Acknowledgements v

Table of Contents vii

List of Tables ix

List of Figures x

Chapter 1: Introduction 1

1.1 Coordination Chemistry 1

1.1.1 Geometry and Structure of Coordination Compounds 1

1.1.2 Strong field and weak field ligands 2

1.1.3 Polydentate ligands 3

1.1.4 Single atom bonding motifs 4

1.1.5 Specialized ligand types 4

1.1.6 Common ligands 5

1.1.7 Electronic Structure of Coordination Compounds 7

1.2 The Potential of Metal Organic Frameworks (MOFs) 8

1.2.1 Efforts of Adding Pollution Control Systems to Vehicles 9

1.2.2 Advanced and Future Technology 12

1.3 Preliminary works (MOF's) 14

Chapter 2: Synthesis and Characterization of Lipid Metal Organic Networks 22

2.1 Molecular design 22

2.2 Synthesis of structural model of LMONs 23

2.1.2 Crystal structure of [C17 H20 N2 O4 Zn (PyPr)] n (1) 24

2.3 Synthesis of Zn- Lmon derivatives 29

Chapter 3: Self-assembly and Thermoplastic Properties of Lipid Metal Organic Networks 34

3.1 Differential scanning calorimeter (DSC) 34

3.2 Thermo gravimetric analysis (TGA) 39

3.3 Dynamic light scattering (DLS) 42

3.4 Self- assembly properties 45

3.5 Post-assembly Modifications 48

Conclusions 50
References 51
Glossary 54
Appendix 55
A.1 SUPPORTING INFORMATION FOR CHAPTER 2 55
A.2 SUPPORTING INFORMATION FOR CHAPTER 3 59
A.2.1 Differential scanning calorimeter (DSC) 60
A.2.2 Thermo gravimetric analysis (TGA) 62
Curriculum Vita 63

List of Tables

Table 1.1: Examples of common ligands 6
Table 1.2: BTC and BTB chemical structures.....20
Table 2.1: Crystal data and structure refinement for Zinc complex 1 27
Table 2.2: Selected bond lengths (Å) and angles (°) for Zinc complex 1 28
Table 2.3: Bidentate ligands were combined to modify the lipid metal organic network.....29
Table 3.1: Shows the Average molecular mass of LMONs. 42

List of Figures

Figure 1.1: Carbon Monoxide levels per year. 10
Figure 1.2: U.S. ambient air quality standards. 11
Figure 1.3: Sulfur effect in low emission vehicles- direct fuel injection engines. 12
Figure 1.4: Effect of fuel sulphur on lean NOx traps flow reactor study. 13
Figure 1.5: Influence of sulphur concentration in gasoline on vehicle after treatment system durability.13
Figure 1.6: Lean NOx adsorber catalyst data. 14
Figure 1.7: Assembly of metal organic framework by the copolymerization of metal ions with organic linker. 15
Figure 1.8: Diamondoid network. 17
Figure 1.9: 2D square grid structure. 18
Figure 1.10: 1D chain is the base to design noncentrosymmetric 19
Figure 2.1: Metal carboxylate bond. M= Transition Metal ion. 22
Figure 2.2 Lipid Metal-Organic Network design. 23
Figure 2.3: View of crystal structure of Zn complex 1 using 4, 4'-trymethylene dipyridine....25
Figure 2.4: 1D crystal structure polymeric zig-zag. 26
Figure 2.5: Synthesis of Zn-complex 2....30
Figure 2.6: Synthesis of Zn-complex 3....31
Figure 2.7: Synthesis of Zn-complex 4....32
Figure 2.8: Synthesis of Zn-complex 5....33
Figure 3.1: Melting point of complex 2 determined by DSC 35
Figure 3.2: Melting point of complex 3 determined by DSC. 35
Figure 3.3: Melting point of complex 4 determined by DSC. 36
Figure 3.4: Melting point of Complex 5 determined by DSC. 36
Figure 3.5: the graph illustrates oxidation induction time of complex 2. 37
Figure 3.6: the graph illustrates Oxidation induction time of complex 3. 37
Figure 3.7: the graph illustrates oxidation induction time of complex 4. 38
Figure 3.8: The graph illustrates oxidation induction time of Complex 5....38
Figure 3.9: TGA curve of complex 2....40
Figure 3.10: TGA curve of complex 3 40
Figure 3.11: TGA curve of complex 4....41
Figure 3.12: TGA curve of complex 5....41
Figure 3.13: DLS of complex 2. 43
Figure 3.14: DLS of complex 3. 43
Figure 3.15: DLS of complex 4. 44
Figure 3.16: DLS of complex 5. 44
Figure 3.17: Optical polarized microscopy. 45
Figure 3.18: XRPD of Zn complex 2. Blue line describes Zinc (II) metal organic polymer, gray line describes melted Zinc (II) Metal Organic Polymer. 46
Figure 3.19: SEM image of Zn complex 2. 47
Figure 3.20: The melting point of Zn complex 6 exhibits a small change indicating cross linking of the olefins. 48
Figure 3.21: IR of Zn-Complex 6 before UV exposure....49
Figure 3.22: IR of Zn-Complex 6 after UV exposure. 49
Figure A.1: XRPD of complex 1. 55
Figure A.2: FTIR of complex 2. 56
Figure A.4: Experimental X-Ray diffraction of complex 3....57
Figure A.5: XRPD of complex 4. 57

Figure A.6: XRDP of complex 5. 58
Figure A.2.1: Synthesis of Zn-complex 6. 59
Figure A.2.2: Melting point of Zn-complex 6. 60
Figure A.2.3: Oxidation induction time of Zn-complex 6. 60
Figure A.2.4: Oxidation induction time of complex 6 after UV exposure. 61
Figure A.2.5: TGA of Complex 6. 62

Chapter 1: Introduction

1.1 COORDINATION CHEMISTRY

Coordination chemistry is the ability of certain ions and molecules to combine in stoichiometric proportions to yield new and more complexes species [8]. The ions or molecules surrounding the metals are called ligands. Ligands are generally bounded to a metal ion by a coordinate covalent bond (donating electrons from a lone electron pair into an empty metal orbital), and are thus said to be coordinated to the ion. The areas of coordination chemistry can be classified according to the nature of the ligands [9].

Organometallic chemistry: ligands are organic (alkenes, alkynes, alkyls) as well as "organic-like" ligands such phosphines, hydride, and CO [9].

Classical: ligands in classical coordination chemistry bind to metals, almost exclusively, via the "lone pairs" of electrons residing on the main group atoms of the ligand. Some typical ligands are H_2O, NH_3, Cl^-, and CN^- [9].

Coordination chemistry focuses on reactivity and properties of complexes containing individual metal atoms or small ensembles of metal atoms [9].

1.1.1 Geometry and Structure of Coordination Compounds

The number of ligands attached to the metal (more specifically, the number of σ-type bonds between ligand(s) and the central atom). Coordination numbers are normally between two and nine, but large numbers of ligands are not uncommon for the lanthanides and actinides. The number of bonds depends on the size, charge and electron configuration of the metal ion and the ligands. Metal ions may have more than one coordination number [9].

Typically the chemistry of complexes is dominated of interactions between s-p molecular orbitals of the ligands and the d orbitals of the metal ions. The s, p, and d orbitals of the metal can accommodate eighteen electrons. The maximum coordination number for a certain metal is thus related to the electronic configuration of the metal ion (more specifically, the number of empty orbitals) and to the ratio of the size of the ligands and the metal ion. Large metals and small ligands lead to high

coordination numbers. Small metals with large ligands lead to low coordination numbers. Due to their large size, lanthanides, actinides, and early transition metals tend to have high coordination numbers [9].

Different ligand structural arrangements result from the coordination number. Most structures follow the points-on-a-sphere pattern (or, as if the central atom were in the middle of a polyhedron where the corners of that shape are the locations of the ligands), where orbital overlap (between ligand and metal orbitals) and ligand-ligand repulsions tend to lead to certain regular geometries [9]. The most observed geometries are:

Linear for two-coordination,

Trigonal planar for three-coordination,

Tetrahedral or square planar for four-coordination,

Trigonal bipyramidal or square pyramidal for five-coordination,

Octahedral (orthogonal) or Trigonal prismatic for six-coordination,

Pentagonal bipyramidal for seven-coordination,

Square antiprismatic for eight-coordination, and

Tri-capped Trigonal prismatic (Triaugmented triangular prism) for nine-coordination.

There are many cases with deviate from regular geometry e.g. due to the use of ligands of different types (which result in irregular bond lengths; the coordination atoms do not follow a points-on-a sphere pattern), due to the size of ligands, or due to electronic effects [9].

1.1.2 Strong field and weak field ligands

In general, ligands are viewed as donating electrons to the central atom. Bonding is often described using the formalisms of molecular orbital theory [10].

Ligands and metal ions can be ordered in many ways, one ranking system focuses on ligand hardness. Metal ions preferentially bind certain ligands; in general, “hard” metal ions prefer weak field ligands, whereas “soft” metal ions prefer strong field ligands [10].

The arrangements of the d orbitals on the central atom (as determined by the strength of the ligand), has a strong effect on virtually all the properties of the resulting complexes. E.g. the energy differences in the d-orbitals have a strong effect on the optical absorption spectra of metal complexes. It turns out that valence electrons occupying orbitals with significant 3d-orbital character absorb in the

400-800 nm region of the spectrum (UV visible range). The absorption of light (what we perceive as the color) by these electrons (that is, excitation of electrons of one orbital to another orbital under influence of light) can be correlated to the ground state of the metal complex, which reflects the bonding properties of the ligands [10].

1.1.3 Polydentate ligands

Many ligands are capable of binding metal ions through multiple sites, usually because the ligands have lone pairs on more than one atom. Ligands that bind via more than one atom are often termed chelating. A ligand that binds through two sites is classified as bidentate, and three sites as tridentate. The bite angle refers to the angle between the two bonds of a bidentate chelate. Chelating ligands are commonly formed by linking donor groups via organic linkers. The classic bidentate ligand is ethylenediamine, which is derived by the linking of two ammonia groups with an ethylene (-CH2CH2-) linker. The number of atoms with which a Polydentate ligand bind to the metal centre is called its denticity, symbolized k^n where n indicates the number non-contiguous donor sites by which a ligand attaches to a metal. In practice, the n value of a ligand is not indicated explicitly but rather assumed. The binding affinity of a chelating system depends on the chelating angle or bite angle [10].

Related to but distinct from denticity is hapticity, symbolized n or eta. Hapticity refers to the number of contiguous atoms in a ligand that are attached to a metal. E.g. butadiene forms both n^2 and n^4 complexes depending on the number of carbon atoms are bonded to the metal. n^n usually refers to unsaturated hydrocarbons and k^n usually to describe Polydentate amine and carboxylate ligands [10].

Complexes of polydentate ligands are called chelate complexes. They tend to be more stable than complexes derived from monodentate ligands. This enhanced stability, the chelate effect, is usually attributed to effects of entropy, which favors the displacement of many ligands by one Polydentate ligand. When the chelating ligand forms a large ring that at least partially surrounds the central atom and bonds to it, leaving the central atom at the centre of a large ring. The more rigid and the higher its denticity, the more inert will be the macrocyclic complex [10].

1.1.4 Single atom bonding motifs

Ambidentate ligands

Unlike polydentate ligands, ambidentate ligand can attach to the central atom in two places but not both. E.g. Thiocyanate SCN^- which can bond at either the sulfur atom or the nitrogen atom. Such compounds give rise to linkage isomerism which is defined as the existence of coordination compounds that have the same composition differing with the connectivity of the metal to a ligand [10]. Polyfunctional ligands can bond to a metal center through different ligand atoms to form various isomers, can also refer to a polydentate ligand that is not fully coordinated to a transition metal [10].

Bridging ligand

Bridging ligand links two or more metal centers. Polyatomic ligands such as CO_2^{2-} are especially prone to bridge. The bonding is complicated because polyatomic ligands are ambidentate and thus the capacity for many different linkage isomers. Atoms that bridge metals are sometimes indicated with prefix of "μ". Most inorganic solids, e.g. $FeCl_2$ are polymers by virtue of the presence of multiple bridging ligands [10].

Metal ligand multiple bond

Metal ligand multiple bonds can bond to a metal center through the same atom but with a different number of lone pairs. The bond order of the metal ligand bond can be in part distinguished through the metal ligand bond angle (M-N-R). This bond angle is often referred to as being linear or bent with further discussion concerning the degree to which the angle is bent. For example, an imido ligand in the ionic form has three lone pairs. One lone pair is used as a sigma N donor; the other two lone pairs are available as L type π donors. If both lone pairs are used in π bonds then the M-N-R geometry is linear [10]. However, if one or both these lone pairs are non-bonding then the M-N-R bond is bent and the extent of the bend speaks to how much π -bonding there may be.

1.1.5 Specialized ligand types

Noninnocent ligands bond with metals in such a manner that the distribution of electron density between the metal center and the ligand is unclear. Describing the bonding of noninnocent ligands often involves writing multiple resonance forms which have partial contributions to the overall state.

Trans spanning ligands are bidentate ligands that can span opposite sites of a complex with square-planar geometry. A wide variety of ligands that chelate in the cis fashion already exist, but very few can link opposite vertices on a coordination polyhedron [10].

1.1.6 Common ligands

Virtually every molecule and ion can serve as a ligand for (or "coordinate to") metals. Monodentate ligands include virtually all anions and all simple Lewis bases. Thus the halides and pseudo halides are important anionic ligand whereas ammonia, carbon monoxide, and water are particularly common charge – neutral ligands. The steric properties of some ligands are evaluated in terms of their cone angles [10].

Beyond the classical Lewis bases and anions, all unsaturated molecules are also ligands, utilizing their pi-electrons in forming the coordinate bond. Also, metals can bind to the sigma bonds. E.g. silanes, hydrocarbons, and dihydrogen [10].

In complexes of non-innocent ligands, the ligand is bonded to metal via conventional bonds, but the ligand is also redox-active [10].

Table 1.1: Examples of common ligands

Ligand	Formula(bonding atoms(s)	Charge	Most common denticity	Remark(s)
Iodide iodo	I^-	monoanionic	monodentate	
Bromide bromo	Br^-	monoanionic	monodentate	
Sulfide thio or bridging thiolate	S^{2-}	dianionic	monodentate (M=S),or bidentate bridging (M-S-M')	
Thiocyanate thiocyanato	S-CN^-	monoanionic	monodentate	ambidentate
Chloride chloro	Cl^-	monoanionic	monodentate	also found bridging
Nitrate	O-NO_2^-	monoanionic	monodentate	
Azide	N-N_2^-	monoanionic	monodentate	
Fluride fluoro	F^-	monoanionic	monodentate	
Hydroxide hydroxo	O-H^-	monoanionic	monodentate	Often found as a bridging ligand
Oxalate	[O-C(=O)-C (=O)-O]$^{2-}$	dianionic	bidentate	
Water aqua	H-O-H	neutral	monodentate	monodentate
Isothiocyanate isothiocyanato	N=C=S^-	monoanionic	monodentate	ambidentate
Acetonitrile	CH_3 CN	neutral	monodentate	
Pyridine	C_5H_5N	neutral	monodentate	
Ammonia ammine	NH_3	neutral	monodentate	

Ethylene diamine	en	neutral	bidentate	
2,2' Bipyridine	bipy	neutral	bidentate	Easily reduced to its (radical) anion or even to its dianion
1,10-Phenanthroline	phen	neutral	bidentate	
Nitrite nitro	$N\text{-}O_2^-$	monoanionic	monodentate	ambidentate
Nitrite nitro	$O\text{-}N\text{-}O^-$	monoanionic	monodentate	ambidentate
Triphenylphosphine	PPh_3	neutral	monodentate	
Cyanide cyano	CN^-	Monoanionic	monodentate	Can bridge between metals (both metals bound to C, or one to C and one to N)
Carbon monoxide carbonyl	CO	neutral	monodentate	Can bridge between metals (both metals bound to C)

1.1.7 Electronic Structure of Coordination Compounds

Many of the properties of metal complexes are dictated by their electronic structures. The electronic structure can be described by a relatively ionic model that ascribes formal charges to the metal and ligands and does not focus on covalency. This approach is the essence of Crystal field theory (CFT). Crystal field theory, introduced by Hans Bethe in 1929, gives a quantum mechanically based attempt at

understanding complex. But crystal field theory treats all interactions in a complex as ionic and assumes that the ligands can be approximated by negative point charges [11-13].

1.2 The Potential of Metal Organic Frameworks (MOFs)

Metal organic framework (MOF) compounds are a relatively new class of nano-porous material that show promise for hydrogen storage applications because of their tunable pore size and functionality and CO_2 capture [14-16].

A research team at the National Institute of Standards and Technology (NIST) used neutron scattering techniques to visualize where hydrogen latches onto the lattices-like arrangement of zinc and oxygen clusters in a particular nanoscale material called MOF5 [14-16].

Taner Yildirim and Michael Hartman found that MOF5 has four types of hydrogen docking sizes, including a surprising three-dimensional network of “nano-cages” that appears to form after other sites load up hydrogen [14-16].

They determine that the metal-oxide cluster is responsible for most of the adsorption while the organic linker plays only a secondary role [14-16].

Yildirim and Hartman found that the two most stable sites in the MOF scaffolding already offer considerable room for storage hydrogen. Earlier studies suggested that at about -200 C MOF5 could hold less than 2% of its weight in hydrogen [14-16].

The NIST research indicates ample room for improvement. At very low temperatures, hydrogen uptake approached 10% of the material’s weight. The bulk of the hydrogen was held in nanometer-scale cavities inside the box-like arrangements of zinc and oxygen clusters [14-16].

The results suggest that MOF materials might be engineered to optimize both the storage of hydrogen and its release under normal vehicle operating conditions [14-16].

Separately, researches at the University of Michigan have developed a new MOF material (MOF-177) that has the highest carbon dioxide capacity of any porous material [14-16].

MOF-177 soaks up 140% of its weight in CO_2 at room temperature and reasonable pressure (32bar) [14-16].

A storage tank filled with MOF-177 could store as much CO_2 as would be stored in nine tanks that do not contain MOFs. By comparison, a tank filled with porous carbon – one of the structure state-of-the-art material for capturing CO_2 in power plant flues – would hold only four tanks worth of CO_2 [14-16].

MOFs can be made in large quantities from low-cost ingredients, such as zinc oxide and terephthalate, which is used in plastic soda bottles. And finding effective, low-cost ways of reducing CO_2 emissions is crucial according to Yaghi [14-16].

Almost every region of the world is using more energy than ever before, and the prediction is that this will continue to increase, not just for petroleum, but also for coal and natural gas. Whenever fossil fuels are burned, CO_2 is released into the atmosphere, with devastating environmental effects that include the melting of the polar ice caps and the changes in ocean acidity. In the United States alone, each person is responsible for generating more than 15 tons of carbon dioxide a year, largely from automobile and power plant emissions [14-16].

1.2.1 Efforts of Adding Pollution Control Systems to Vehicles

Urban air quality has improved dramatically over the past 20 years. Figure 1.1 shows the declining trend lines for the maximum hourly concentrations of three air pollutants – ozone, carbon monoxide, and nitrogen dioxide – in California [17].

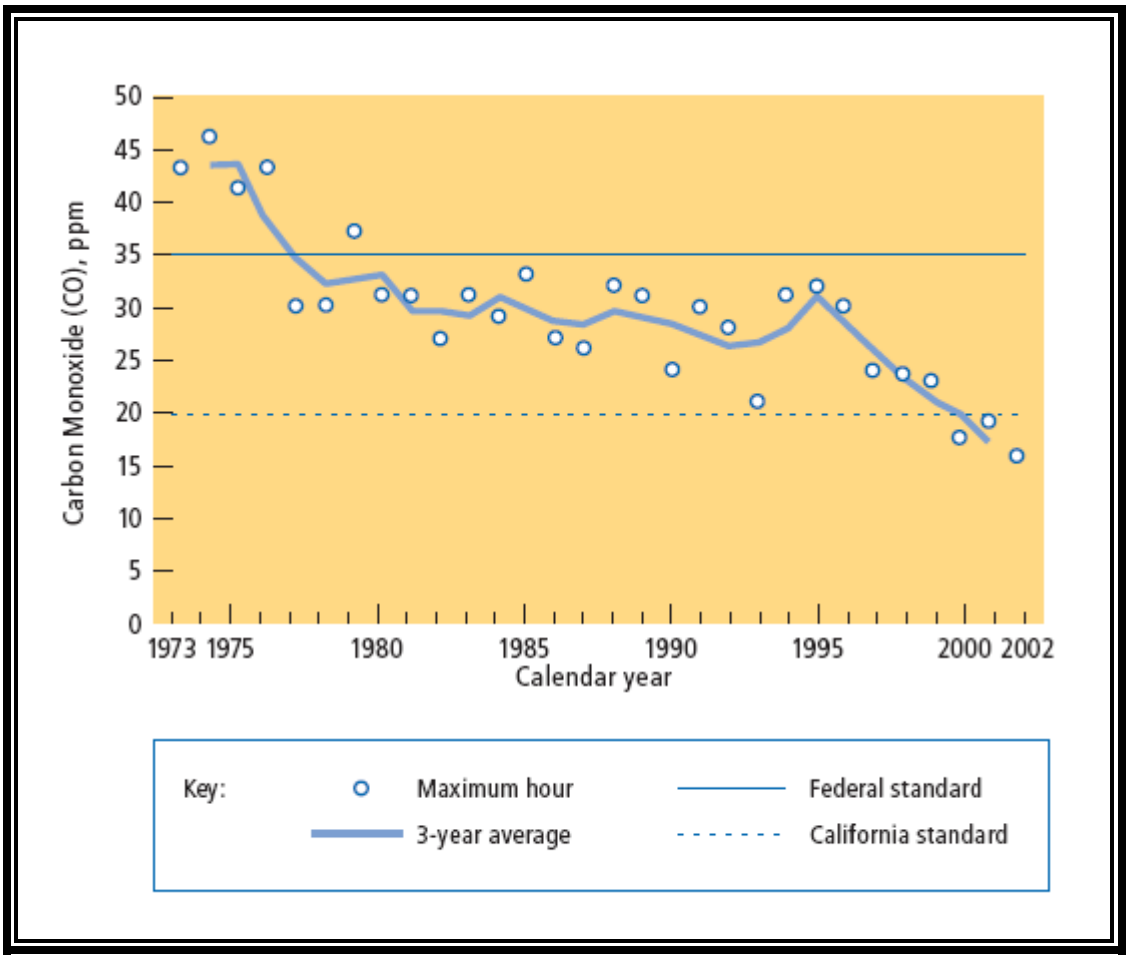

Figure 1.1: Carbon Monoxide levels per year.

The fact of these decrease are not uniform from year to year is a result of annual variation of the weather (meteorology) on ambient pollutant concentrations [17].

The improvement in urban air quality is due to significant reductions in emissions from the various emissions source categories such as factories, power plants, consumer products, and automobiles. For example, today a new-model passenger car emits less than one percent of volatile organic compounds, less than five percent of the carbon monoxide, and only about 7 percent of the oxides of nitrogen emitted by a vehicle built before emissions controls began to be used. Similarly impressive improvements have been achieved for other emissions source categories [17].

The introduction of reformulated gasolines also has helped improve air quality. Federal phase I gasoline was introduced in January 1995, Phase II in January 2000. California Phase 2 reformulated gasolines was required in California mid-1996 and Phase 3 introduced at the end of 2003. Federal Phase II and California Phases 2 and 3 reformulated gasolines are believed to reduce ozone-forming emissions from cars and light trucks by about 10 to 15 percent. It is difficult to discern this effect in Figure 1.2 because of the year-to-year variability caused by other factors, such as meteorology [17].

Some of the criteria pollutants, like carbon monoxide, are primary pollutants, which are emitted directly by identifiable sources. Others, like ozone, are secondary pollutants, which are formed by reactions in the atmosphere. And others, like particulates, are of mixed origin. Figure 1-2 lists the criteria pollutants and their federal limits [17]

Criteria Pollutant	Averaging Time	Maximum Average Concentration	
		Federal Standard	California Standard
Ozone; ppm	1-hour 8-hour	0.12 0.08	0.09 —
Carbon monoxide (CO), ppm	1-hour 8-hour	35 9	20 9.0
Nitrogen dioxide (NO_2), ppm	1-hour Annual	— 0.053	0.25 —
Sulfur dioxide (SO_2), ppm	1-hour 24-hour Annual	— 0.14 0.03	0.25 0.04 —
Suspended particulate matter (PM_{10}), $\mu g/m^3$	24-hour Annual	150 50	50 20
Suspended particulate matter ($PM_{2.5}$), $\mu g/m^3$	24-hour Annual	65 15	— 12
Lead, $\mu g/m^3$	30-day Quarterly	— 1.5	1.5 —
Sulfates, $\mu g/m^3$	24-hour	—	25
Hydrogen sulfide, ppm	1-hour	—	0.03
Vinyl chloride, ppm	24-hour	—	0.01

Figure 1.2: U.S. ambient air quality standards.

1.2.2 Advanced and Future Technology

Manufacturers are working toward ambitious goals for improved fuel consumption/reduced CO2 emissions. Operation at lean air-fuel ratio is the most promising means to achieve these reductions in gasoline powered vehicles. However, lean operation introduces a new challenge for exhaust emission control. While existing catalysts effectively remove unburned HC and CO during lean operation, then remove NOx only during stoichiometric or rich operation [18].

Many manufacturers are developing and introducing lean-burn engines that have the potential to reduce fuel consumption by up to 15 to 20%. These engines, however, require NOx control technologies that can function under lean conditions. These technologies are very sensitive to fuel sulphur [18].

Figures 1.3 and 1.4 provide examples of the adverse effect of sulphur on storage type NOx reduction catalyst needed in lean burn vehicles. With increased exposure time, the lower sulphur gasolines allow catalysts to retain a higher NOx conversion efficiency. Further tests in vehicles (Figures 1.5 and 1.6) confirm the critical need for very low sulphur gasolines. Sulphur –free gasolines are required to achieve and maintain high NOx conversion efficiencies [18].

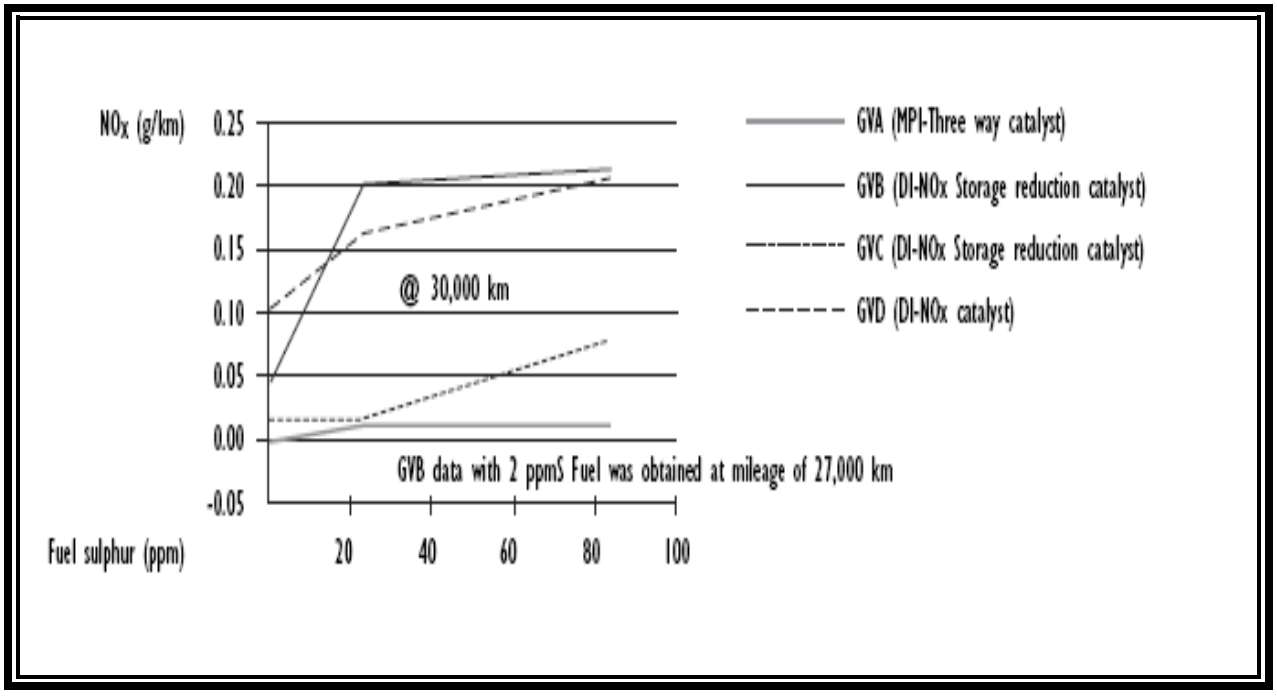

Figure 1.3: Sulfur effect in low emission vehicles- direct fuel injection engines.

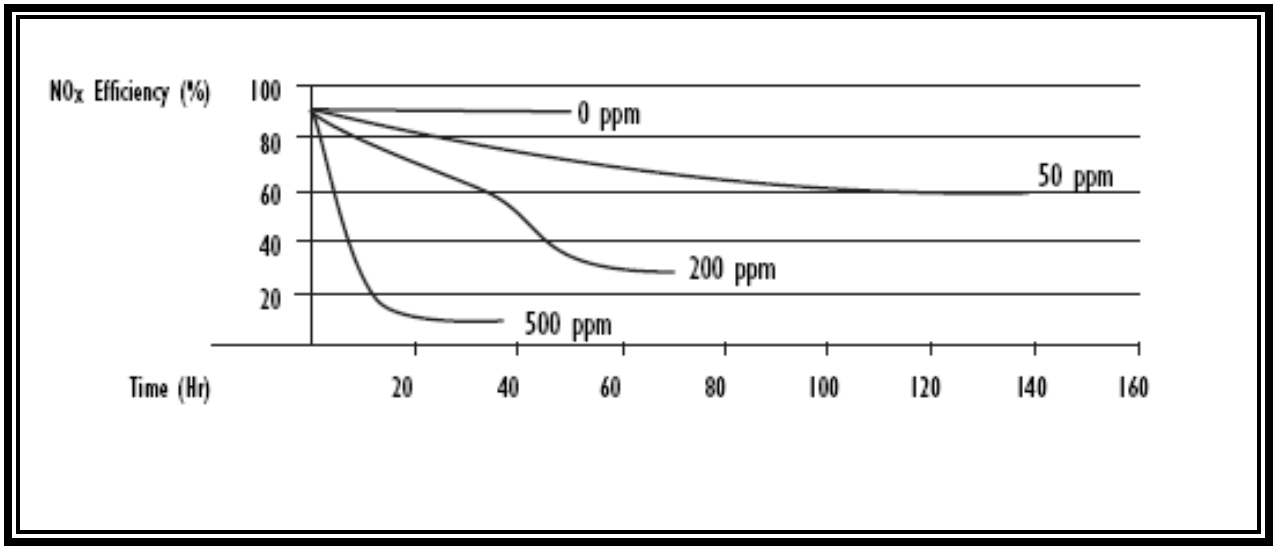

Figure 1.4: Effect of fuel sulphur on lean NOx traps flow reactor study.

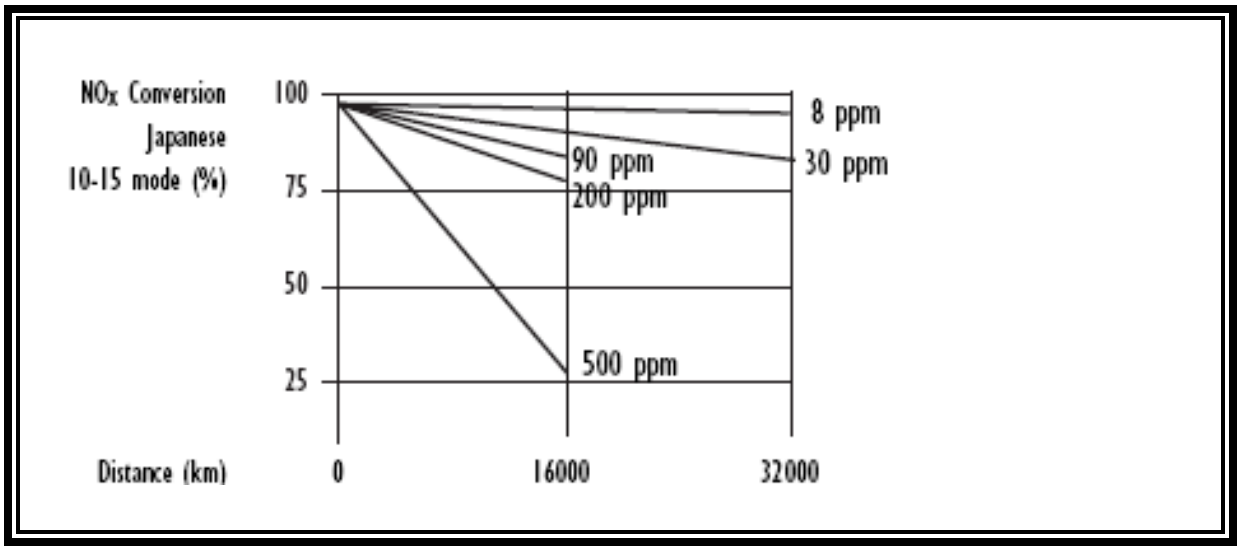

Figure 1.5: Influence of sulphur concentration in gasoline on vehicle after treatment system durability.

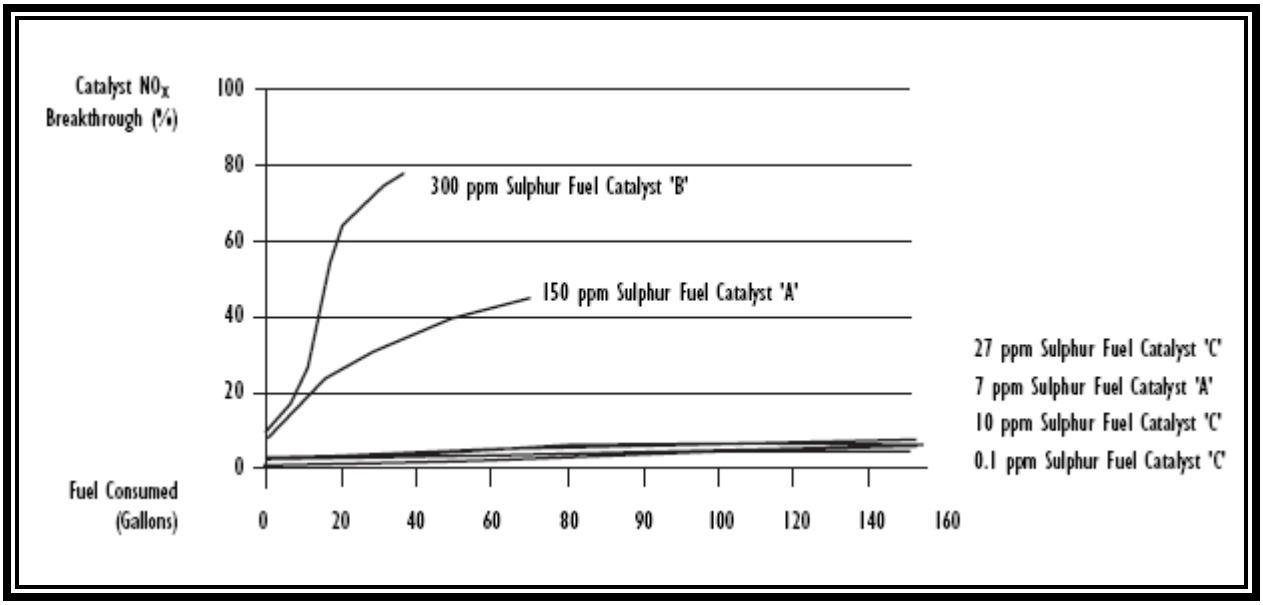

Figure 1.6: Lean NOx adsorber catalyst data.

1.3 Preliminary works (MOF's)

The purpose of this thesis work is intended to design and synthesize metal monodentate lipid compounds and ditopic bridging ligands leading to a new class of robust porous networks. The assembly of metal organic networks by the copolymerization of metal ions with organic linkers to give flexible metal bipyridine structures with expanded diamond topology and rigid metal carboxylate clusters that can be linked by benzene to form rigid extended networks in which the M – O – C core referred as a secondary building unit of each cluster acts as a large octahedron decorating a 6-connected vertex in a cube as is shown in figure 1.7 [19].

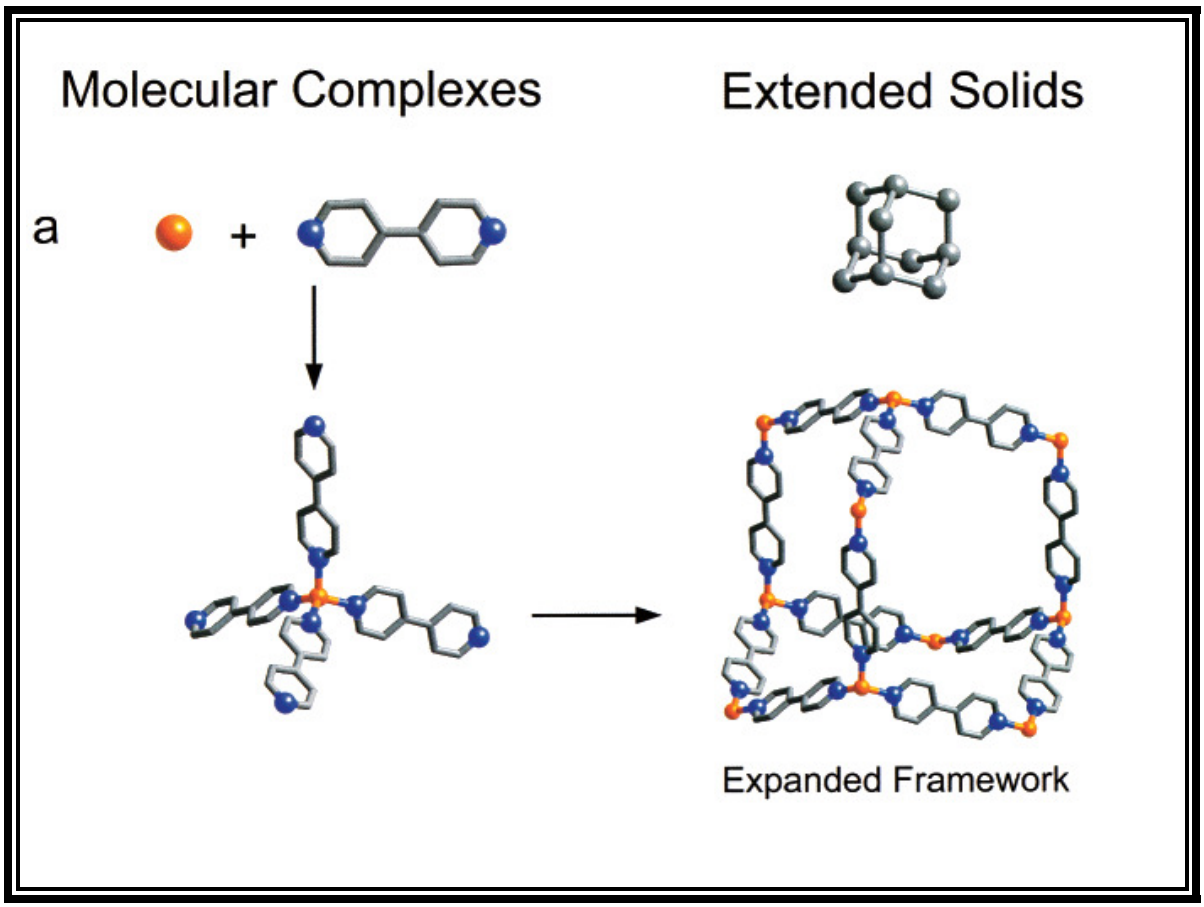

Figure 1.7: Assembly of metal organic framework by the copolymerization of metal ions with organic linker.

Secondary building units (SBUs) are molecular complexes and cluster entities in which ligand coordination modes and metal coordination environments can be utilized in the transformation of these fragments into extended porous networks using polytopic linkers [19].

The work of Mohamed Eddaoudi et. al. title as “Modular Chemistry: Secondary Building Units as a Basis for the Design of Highly Porous and Robust Metal-Organic Carboxylate Frameworks” is focused on the successful use of secondary building units in the formation of certain predicted structures and its impact on identifying networks with optimal porosity and the ability to design the structures as allowed the synthesis of compositions with designed pore structure (size, shape and function) [19-37].

Namely, (a) the important process of functionalizing the pores with useful molecular moieties that introduce weaker and reversible interactions (complex function) into such open frameworks, (b) the assembly and use of less symmetric SBUs including chiral ones and (c) the design of dimensionally larger SBUs that still have a small number (3-6) of points of connection allowing them to be incorporated into open frameworks [19].

According to Owen R Evans and Wenbin Lin [38] it is known that coordination bonds can be utilized to counteract unfavorable centrosymmetric intermolecular interactions in the solid state. Noncentrosymmetric coordination networks with desired topologies can be rationally designed by taking advantage of well-defined metal coordination geometries in combinations with carefully chosen rigid bridging ligands. Owen and Lin describe their successful development of several crystal-engineering strategies toward the synthesis of noncentrosymmetric coordination networks and preliminary evaluation of their second-order nonlinear optical (NLO) properties. This work was divided in three sections on the basis of dimensionality coordination networks: specifically, three-dimensional (3D) diamondoid networks, two-dimensional (2D) grid structures, and one-dimensional (1D) and related helical systems [38].

3D Diamondoid Networks. The most obvious choice of 3D networks for crystal engineering of noncentrosymmetric solids is the diamondoid network (DN) figure 1.8 [38].

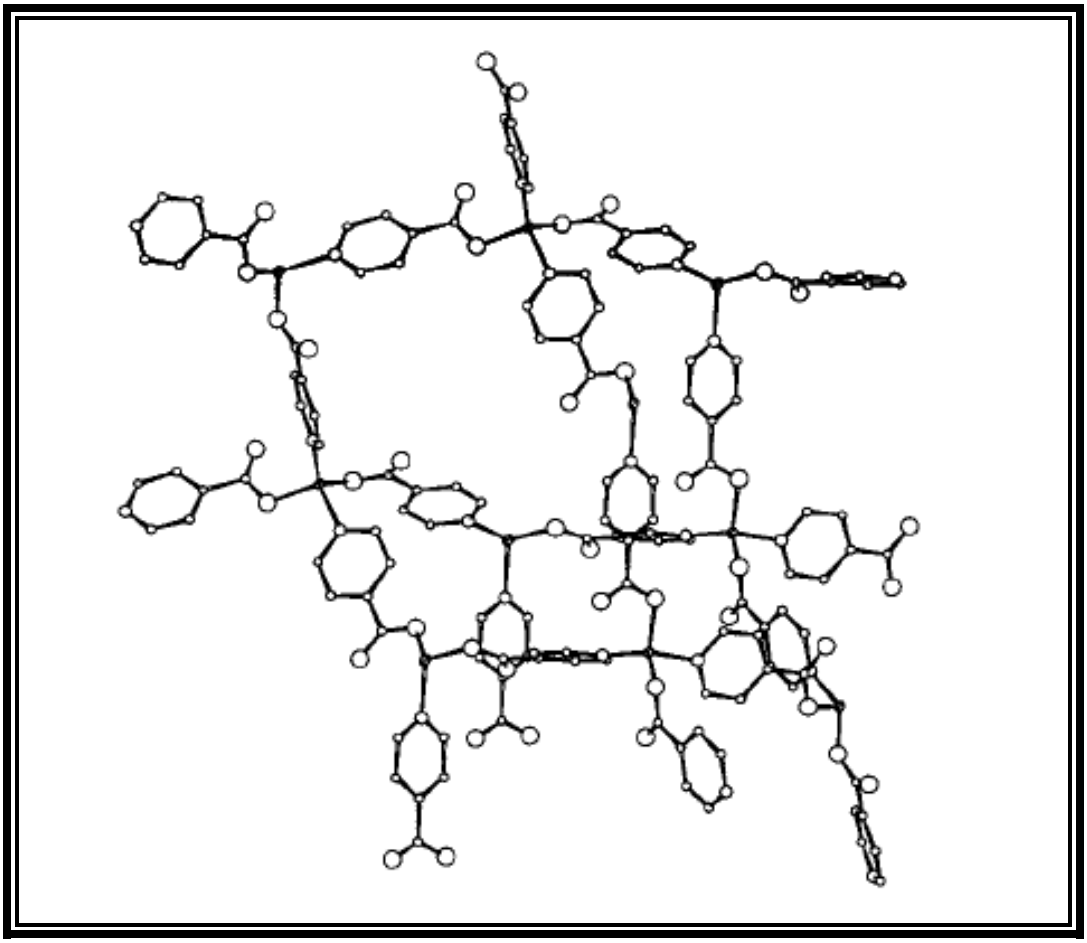

Figure 1.8: Diamondoid network.

2D Coordination Networks. Owen R Evans and Wenbin Lin hypothesize that the bent configuration of an M-pyridinecarboxylate ligand can accommodate the metal centers to adopt infinite 2D grid structures figure 1.9 [38].

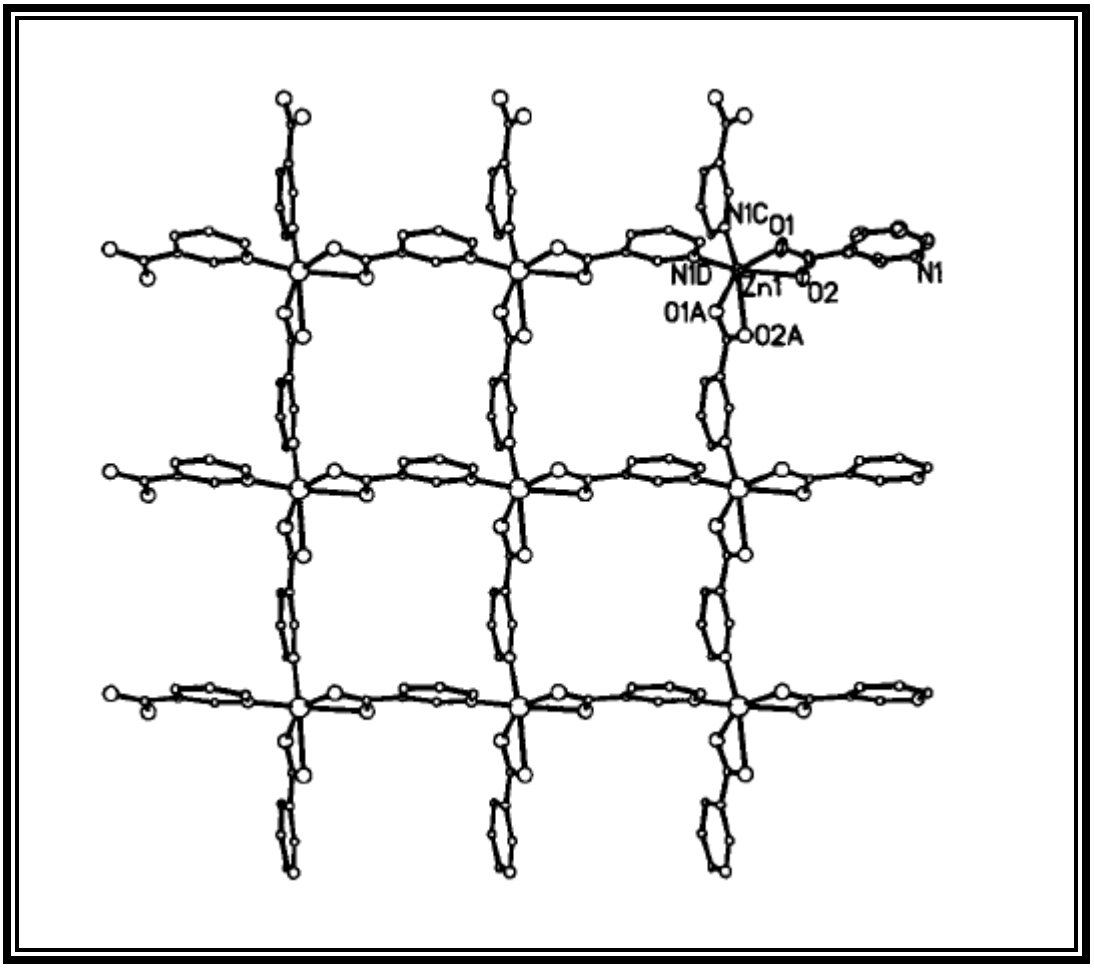

Figure 1.9: 2D square grid structure.

1D and Related Helical Coordination Networks. The design of noncentrosymmetric 1D chains can be readily achieved, but construction of a noncentrosymmetric solid based on 1D chain can be a formidable task owing to the lack of control in two other dimensions figure 1.10 [38].

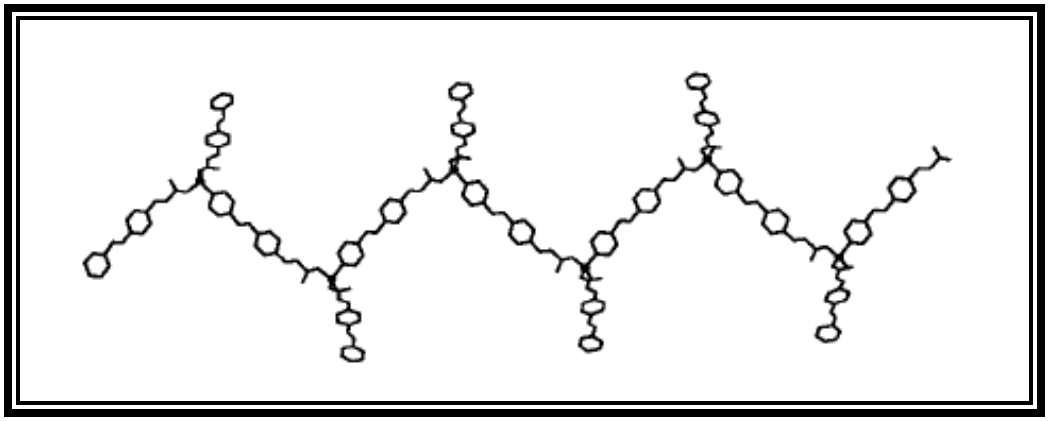

Figure 1.10: Design of noncentrosymmetric 1D chain.

Jaheon et. al. described an approach having significant implications for the design of highly porous and robust MOF structures for which the rigid of the SBUs made it possible to predict the topology [39]. They illustrate using nine new MOFs assembled from a diverse set of large organic linkers and divalent transition metal ions, that this strategy can be generally applied to understanding, determining, and predicting new structure patterns and topologies of complex MOF structures. Although the compounds in this study have structures that offer promising host-guest chemistry and porosity, already investigated for the other MOFs the main focus in the work of Jaheon et. al. is the understanding of structural aspects relating to their construction from SBUs. They also show that SBUs with less symmetric and uncommon shapes can lead to new structure types [39].

As a result of this approach structures can be understood by considering a vertex in a network that can be replaced by more than one vertex to give a decorated network. Extended framework in which $In_{10}\ S_{18}^{10-}$ units occupy the position of 4-connected C atoms in the diamond network. The new cluster of vertex is referred to as a SBU. The special case when a vertex in an n-connected network is replaced by n vertexes is called augmentation [39].

Frameworks with large pores can be created if vertexes in a network are space apart by longer links to give expanded structures. Polytopic organic links can also function as a decorated and/or expanded vertex to produce organic SBUs: Thus, the 1,3,5-C atoms in BTC (Benzenetricarboxylate) and in the central benzene ring of BTB (Benzenetribenzoate) decorate at three connected vertex, because

these atoms form a triangular SBU that can be linked to other shapes [39]. The 2-connected benzoate rings in BTB space apart the central benzene ring from the carboxylate carbon atoms; thus, BTB is considered an expanded version of BTC [39]. Table 1.2 describes the chemical structures of BTC and BTB compounds.

Table 1.2: BTC and BTB chemical structures

Chemical Structure	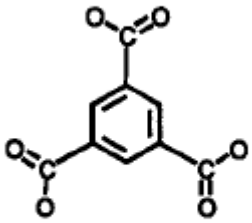 BTC	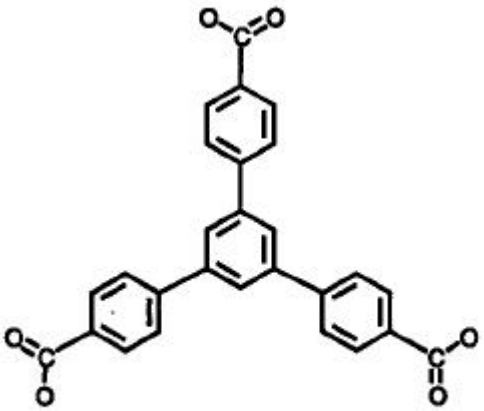 BTB
Name	Benzenetricarboxylate	Benzenetribenzoate

These range and variety of self assembled inorganic structures that can be constructed relies in various types of polymeric structures include 1-D, 2-D and 3-D network structures. As is mentioned at the beginning of this research the combination of monodentate lipids with Zinc catalyst compounds using different bridges to obtain lipid metal complexes as well as observe and characterize their chemical behavior provides the opportunity to define and understand 1D structures units and coordination arrays .

One-dimensional (1D) chain-like complexes, being the simplest topological type of coordination array, represent a good starting point to model and investigate infinite, polymeric compounds to develop strategies for engineering supramolecular polymers [41]. The relative simplicity of the 1D chain allows the classification of all types of non-covalent contacts between each polymeric super molecule. For example models of structural effects and interactions in diamondoid frameworks [42] involve viewing the 3D frameworks as a number of connected 1D arrays (1D infinite helices or aromatic stacks) and then interpreting the changes in these 1D units. These examples of the controlled engineering of 3D polymers stress the necessity for precise understanding of the design principles for 1D coordination polymers before one can start to rationalize solid-state structures with higher dimensionality [42].

Chapter 2: Synthesis and Characterization of Lipid Metal Organic Networks

The synthesis and characterization of the lipid metal organic networks (LMON) developed in this investigation will be presented in this chapter. The first part of this chapter gives a description of the molecular design of new LMONs. The second part describes the synthesis of a model system that was used to characterize the molecular structure with atomic resolution. The third part describes the synthesis of a family of LMONs that vary their molecular structure systematically.

2.1 MOLECULAR DESIGN

The newly developed LMON here presented were designed based on the intrinsic chemical properties of carboxylic acid groups with transition metal ions, which form coordination bonds with each other (Figure 2.1).

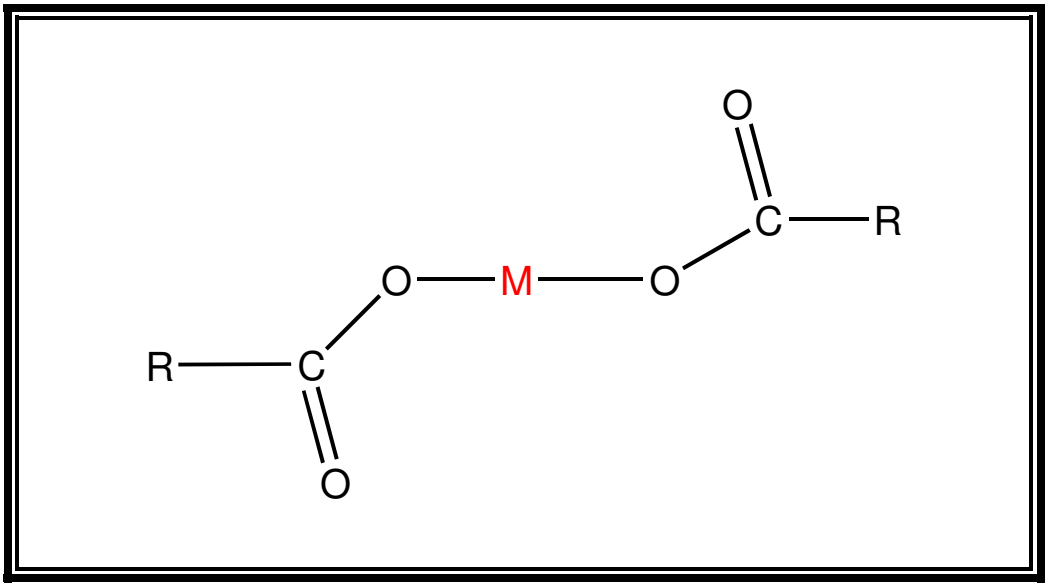

Figure 2.1: Metal carboxylate bond. M= Transition Metal ion.

Ditopic ligands such as 4, 4'-trimethylenedipyridine were used as spacers groups that bridged the transition metal ions that were bonded to the carboxylic acid groups' figure 2.2. In this way, one-dimensional coordination polymers may be obtained. We postulated that this new type of LMON may have interesting physical properties when using biomass-derived fatty acids.

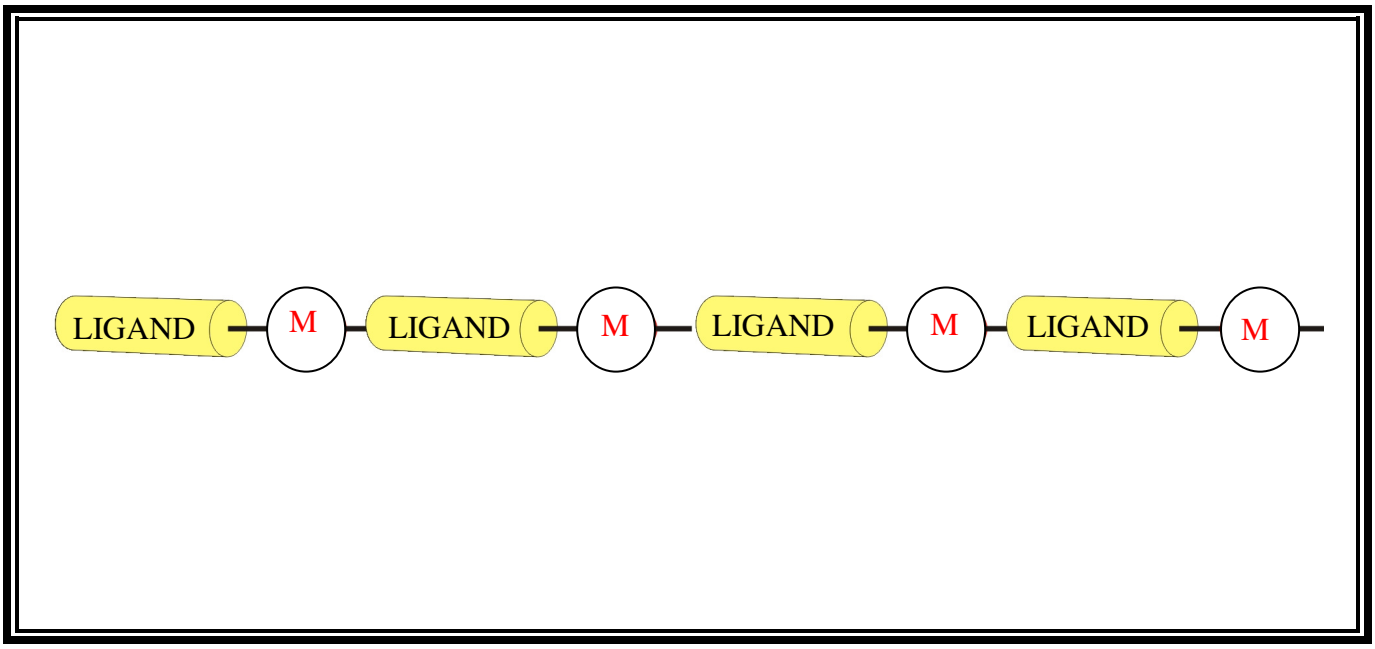

Figure 2.2 Lipid Metal-Organic Network design.

2.2 SYNTHESIS OF STRUCTURAL MODEL OF LMONS

In order to demonstrate the validity of our structural design, we prepared the Zn-complex [C17 H20 N2 O4 Zn (PyPr)] n (**1**). This complex was formulated using two equivalents of acetate and one of 4, 4'-trimethylene dipyridine. The synthesis of this complex was achieved by mixing zinc(II) triflate, where triflate = trifluoromethanesulfate, acetic acid, and 4,4'-trimethylenedipyridine in dimethyl formamide (DMF) and allowed to react under reflux conditions for 18 h. Afterwards, the reaction was cool down and a white microcrystalline precipitate was isolated by filtration and washed with methanol. The same product was obtained when starting with zinc (II) acetate.

2.1.2 Crystal structure of [C17 H20 N2 O4 Zn (PyPr)] n (1)

The Zn-complex 1 was characterized via X-ray crystallography. Single-crystals of **1** were obtained by diethyl ether evaporation into a solution of **1** in DMF. The bidentate ligand 4, 4' trymethylene dipyridine was used to create the crystal structure figure 2.3 and a 1D unit figure 2.4.

The molecule has a rotation angle 172.06^{o} trans and gauche 55.25^{o}. The bite angle is about 127.80^{o}. The ligand which is a bidentate ligand may be represented as a bite angle 127^{o} and 96^{o} for ligand –metal –ligand (L-M-L) with the acetate ligand blocking the other coordination side of the metal. The dihedral angle is around 98° which describes the relation between one metal, the ligand and the repetitive unit. The geometry around the coordination metal is octahedral. The distance from metal center and oxygen is approximately 2.21 Å and the metal Nitrogen bond is approximately 2.09 Å.

The crystal package is a system of polymeric chains in one direction and other perpendicular to this.

The schematic of unit cell is represented in figure 2.4. The crystal, structures and angles of Zn-complex 1 are summarized in tables 2.1 and 2.2.

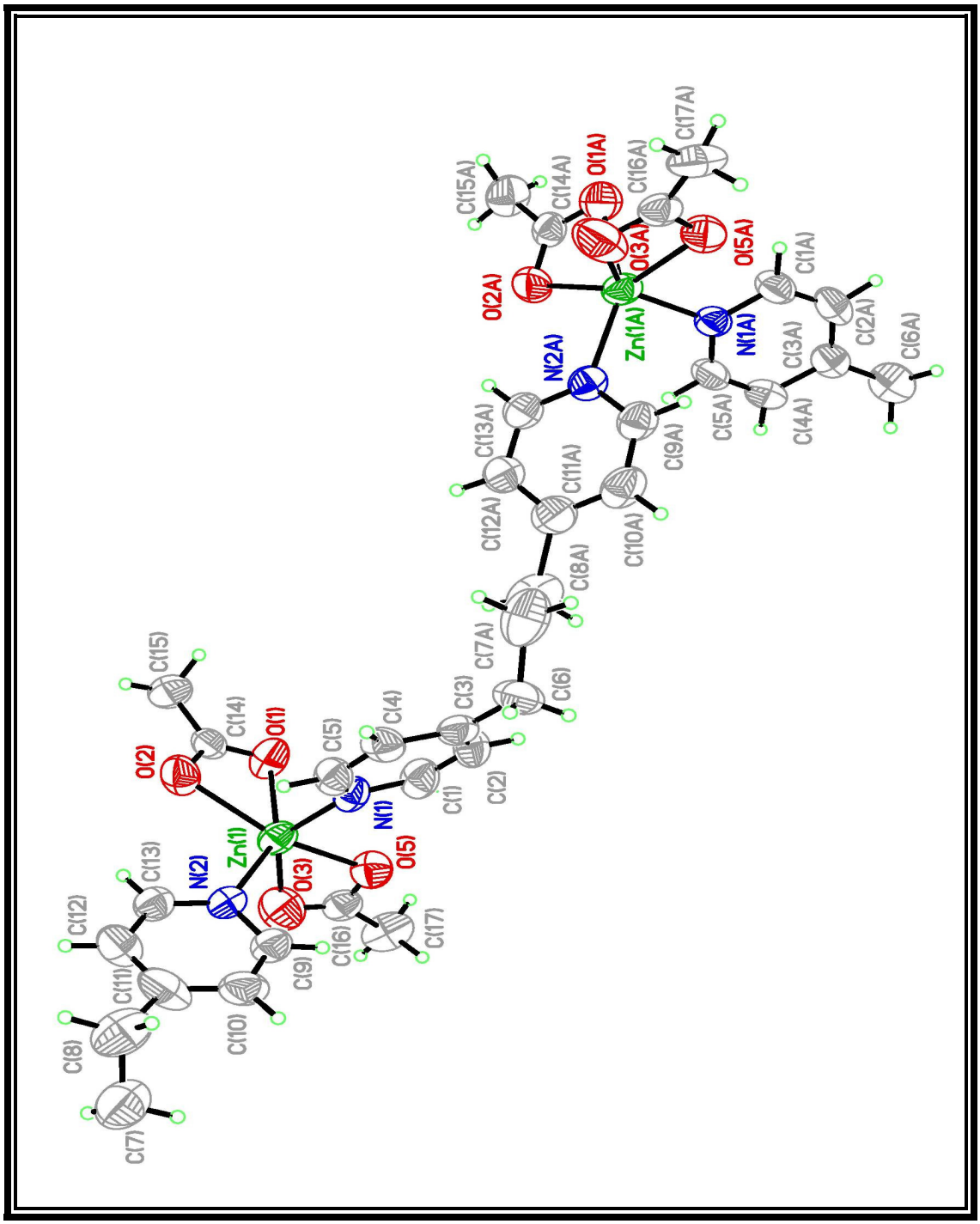

Figure 2.3: View of crystal structure of Zn complex 1 using 4, 4'-trymethylene dipyridine

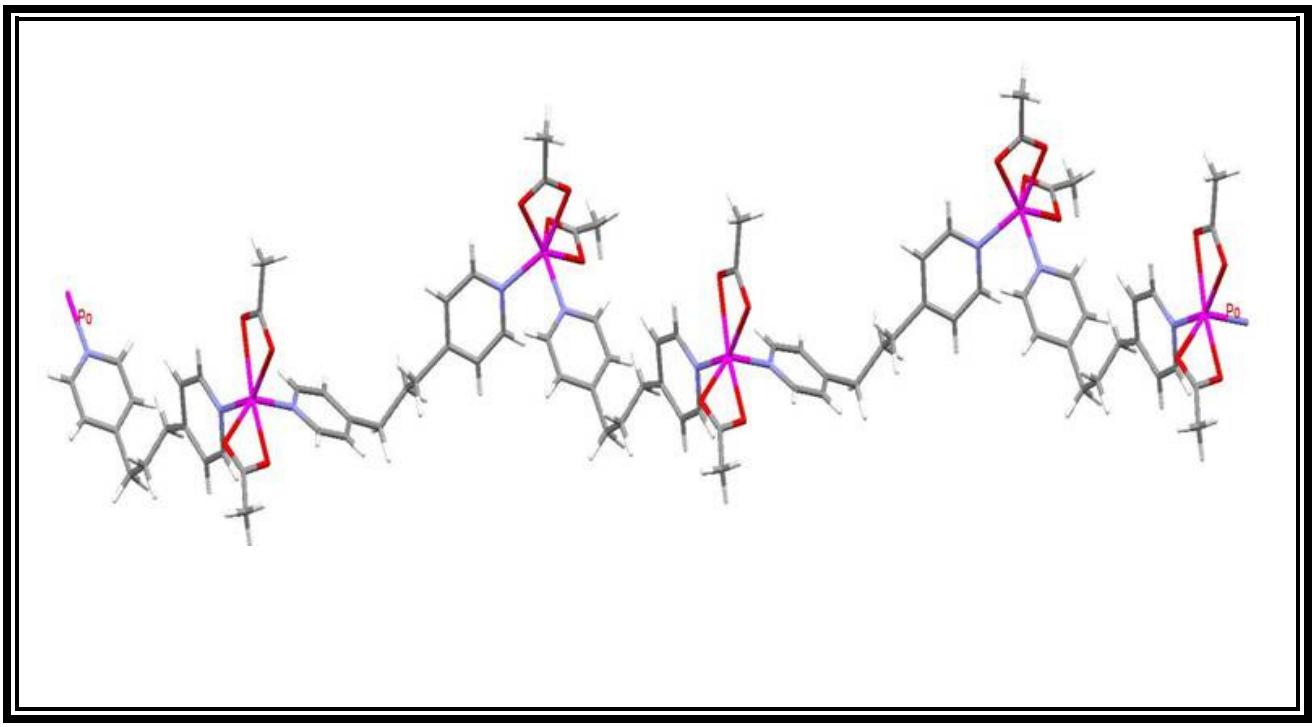

Figure 2.4: 1D crystal structure polymeric zig-zag.

Table 2.1: Crystal data and structure refinement for Zinc complex 1

Identification code	Zinc Complex 1	
Empirical formula	C17 H20 N2 O4 Zn	
Formula weight	381.72	
Temperature	298(2) K	
Wavelength	0.71073 Å	
Crystal system	Orthorhombic	
Space group	Pbcn	
Unit cell dimensions	a = 13.8908(13) Å	α= 90°.
	b = 17.1915(16) Å	β= 90°.
	c = 14.6185(13) Å	γ = 90°.
Volume	3491.0(6) $Å^3$	
Z	8	
Density (calculated)	1.453 Mg/m^3	
Absorption coefficient	1.429 mm^{-1}	
F(000)	1584	
Theta range for data collection	1.88 to 26.80°	
Index ranges	-17<=h<=17, -21<=k<=21, -18<=l<=18	
Reflections collected	36990	
Independent reflections	3736 [R(int) = 0.1220]	
Completeness to theta = 26.80°	100.0 %	
Absorption correction	None	
Refinement method	Full-matrix least-squares on F^2	
Data / restraints / parameters	3736 / 0 / 239	
Goodness-of-fit on F^2	1.042	
Final R indices [I>2sigma(I)]	R1 = 0.0683, wR2 = 0.1727	
R indices (all data)	R1 = 0.1109, wR2 = 0.1942	
Largest diff. peak and hole	0.661 and -0.410 $e.Å^{-3}$	

Table 2.2: Selected bond lengths (Å) and angles (°) for Zinc complex 1

Zn(1)-N(1)	2.086(4)
Zn(1)-N(2)	2.099(4)
Zn(1)-O(5)	2.14(2)
Zn(1)-O(3)	2.162(5)
Zn(1)-O(1)	2.215(4)
Zn(1)-O(2)	2.218(3)
N(1)-Zn(1)-N(2)	96.11(14)
N(1)-Zn(1)-O(5)	85.6(3)
N(2)-Zn(1)-O(5)	117.5(3)
N(1)-Zn(1)-O(3)	137.26(17)
N(2)-Zn(1)-O(3)	92.96(15)
O(5)-Zn(1)-O(3)	53.6(3)
N(1)-Zn(1)-O(1)	97.12(14)
N(2)-Zn(1)-O(1)	149.72(14)
O(5)-Zn(1)-O(1)	90.6(3)
O(3)-Zn(1)-O(1)	95.57(16)
N(1)-Zn(1)-O(2)	105.55(14)
N(2)-Zn(1)-O(2)	92.28(13)

2.3 SYNTHESIS OF ZN- LMON DERIVATIVES

Derivatives of the Zn-complex 1 having fatty acids such as octadecanoic acid was prepared following a similar procedure to 1. All Chemicals used to prepare the reactions grade 99% purity purchased from Sigma – Aldrich were used as received. The following table 2.3 describes the derivatives obtained for LMON.

Table 2.3: Bidentate ligands were combined to modify the lipid metal organic network.

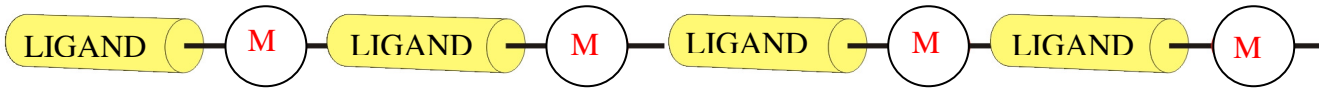

Ligand Variation			
Rigid	**Complex #**	**Flexible**	**Complex #**
4,4’ Dipyridyl 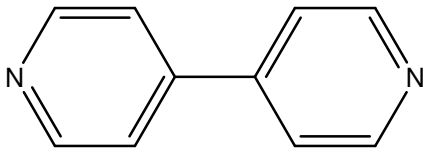	**2**	4,4’Trymethylene dipyridine 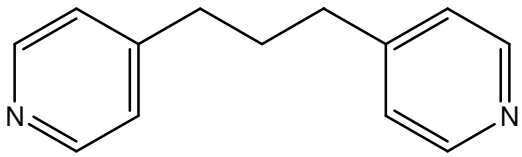	**3**
Di-pyridin-4-yl-diazene 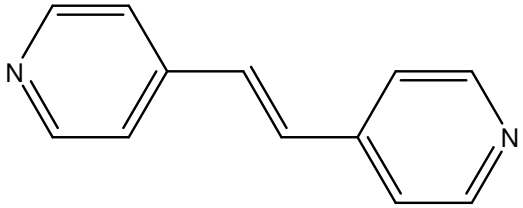	**4**	4,4’-dipyridil ethylene diamide 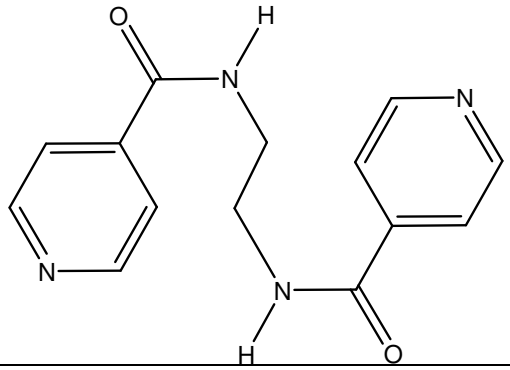	**5**

The derivative of 4, 4'-dipyridil (complex 2) was synthesized by reacting Zinc Trifluoromethane Sulfonate 0.319g, 4, 4'-dipyridil 0.273g and octadecanoic acid 0.5g dissolved in DMF and DEF the reaction was left in reflux approximately 2 hours. The molecular weight of repetitive unit was 786.5. The calculated percentage by mass was C=70.2460%, H=9.995%, N=3.5617%, O=8.1364%, and Zn=8.3137, and the reaction yield percentage was 19.84%. The reaction is illustrated in figure 2.5.

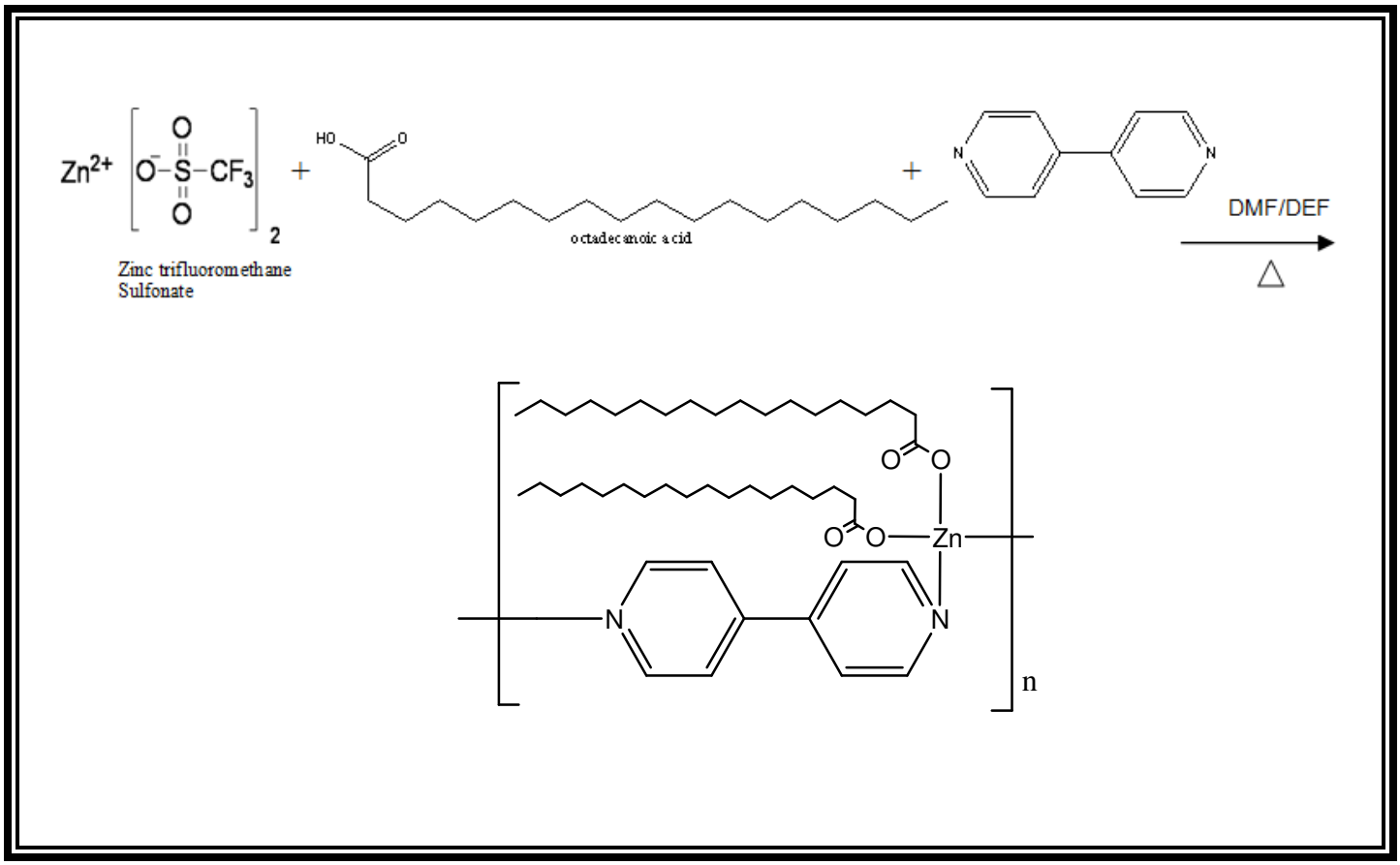

Figure 2.5: Synthesis of Zn-complex 2

The derivative of 4, 4'-trymethylene dipyridine (complex 3) was synthesized by reacting Zinc Trifluoromethane Sulfonate 0.319g, 4, 4'-trymethylene dipyridine 0.348g and octadecanoic acid 0.5g dissolved in DMF and DEF the reaction was left in reflux approximately 2 hours. The molecular weight of repetitive unit was 845.63. The calculated percentage by mass was C=71.0180%, H=10.3694%, N=3.3127%, O=7.5678%, and Zn=7.7326%, and the reaction yield percentage was 43.11%. The reaction is illustrated in figure 2.6. The crystal was prepared using one equivalent of zinc acetate and one equivalent of 4, 4'-trymethylene dipyridine dissolved in ACN. The reaction was left in reflux approximately 3 hours. The solution was separated in a vial with ether diffusion at room temperature.

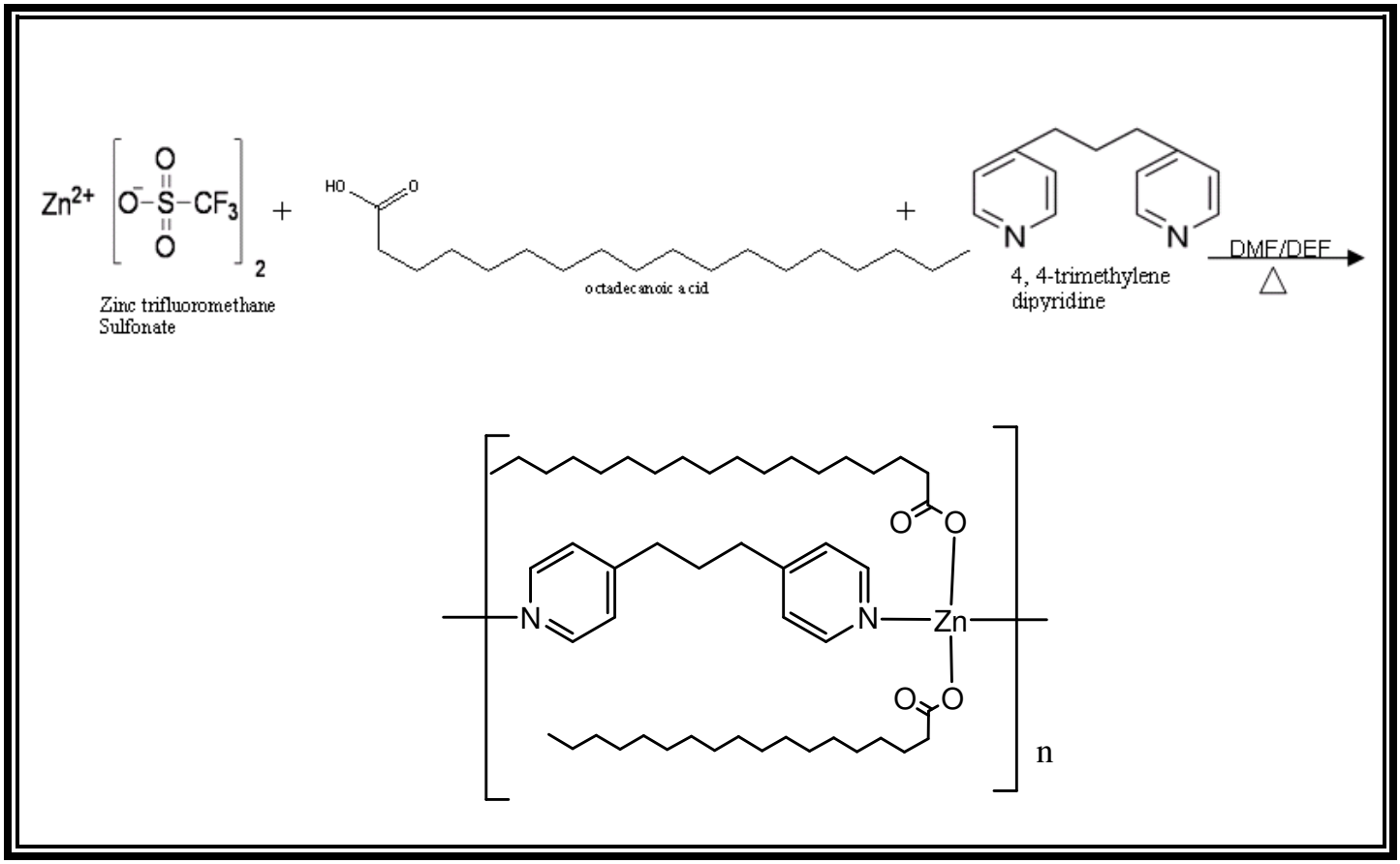

Figure 2.6: Synthesis of Zn-complex 3

The derivative of Di-pyridin-4-yl-diazene (complex 4) was synthesized by reacting Zinc Trifluoromethane Sulfonate 3g, Di-pyridin-4-yl-diazene 1.5g and octadecanoic acid 4.7g dissolved in 20 ml DMF and 5 ml of DEF the reaction was left in reflux approximately 6 hours. The molecular weight of repetitive unit was 814.55. The calculated percentage by mass was C=70.7787%, H=9.8989%, N=3.4391%, O=7.8566%, and Zn=8.0277%, and the reaction yield percentage 34.97%. The reaction is illustrated in figure 2.7

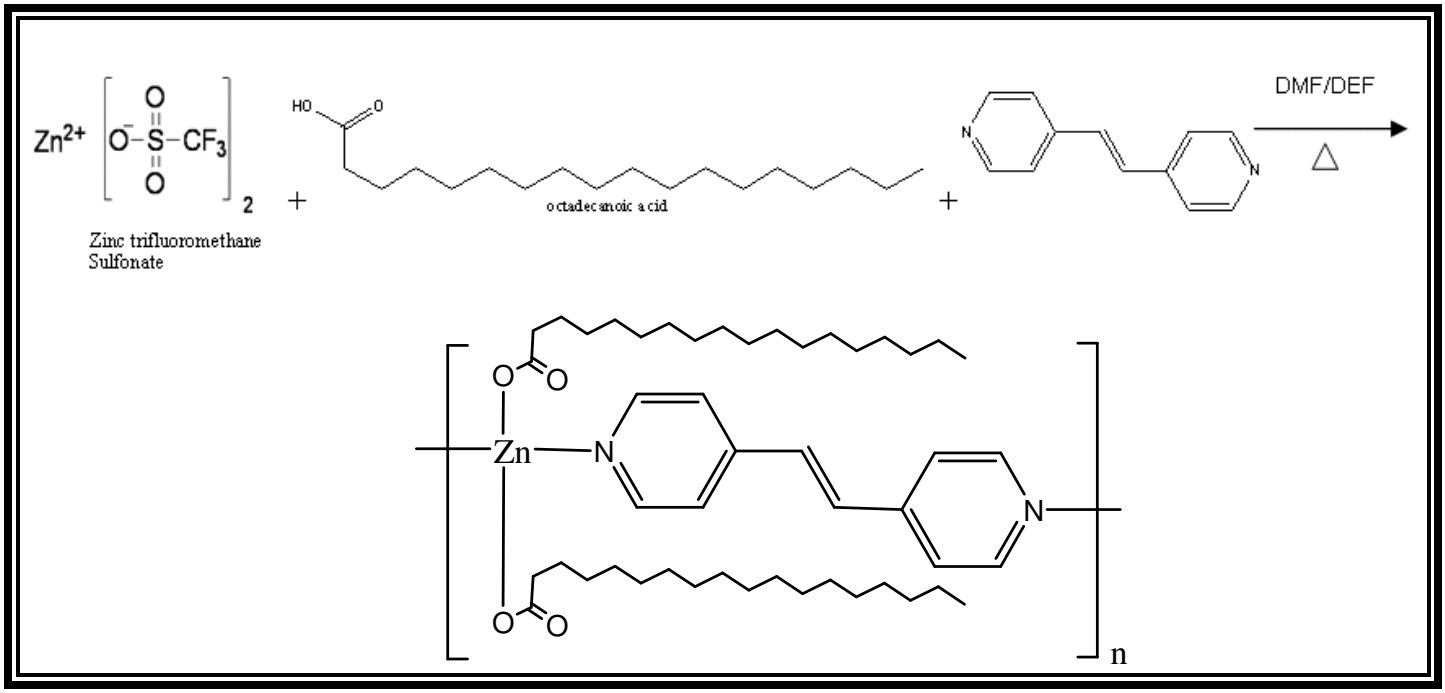

Figure 2.7: Synthesis of Zn-complex 4

The derivative of amide ligand (complex 5) was synthesized by reacting Zinc Trifluoromethane Sulfonate 2.689g, 4, 4-Dipyridil ethylene diamide 2.0g and octadecanoic acid 4.20g dissolved in 20 ml of DMF the reaction was left in reflux approximately 24 hours. The molecular weight of repetitive unit was 902.62. The calculated percentage by mass was C=66.5340%, H=9.3797%, N=6.2074%, O=10.6350%, and Zn=7.2444%, and the yield percentage was 29.94%. The reaction is illustrated in figure 2.8. The crystal was prepared using one equivalent of zinc trifluoromethane and one equivalent of amide dissolved in DMF. The reaction was left in reflux approximately 24 hours. The solution was separated in a vial with ether diffusion at room temperature.

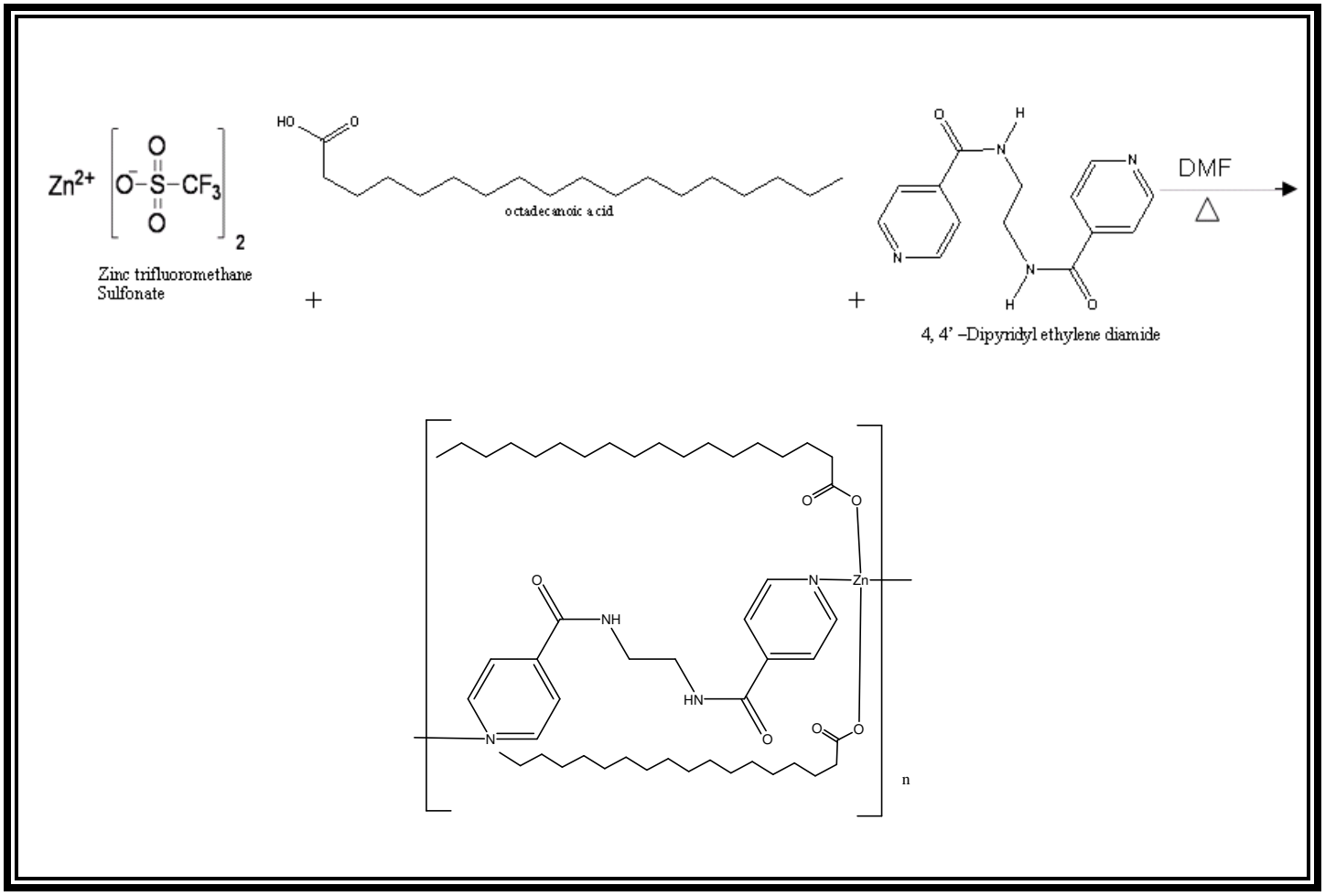

Figure 2.8: Synthesis of Zn-complex 5.

Chapter 3: Self-assembly and Thermoplastic Properties of Lipid Metal Organic Networks

The physical and self-assembly properties of Zn-complexes 2 – 5 were characterized using Thermo gravimetric methods, Differential scanning calorimeter (DSC), polarized optical microscopy, X-ray Powder Diffraction, Infrared Spectroscopy, Dynamic Light Scattering, and Scanning Electron Microscopy.

3.1 DIFFERENTIAL SCANNING CALORIMETER (DSC)

Differential scanning calorimeter (DSC) was used to observe the energy changes that occur as matter transitions from phase to phase. Typically, we observed solid to a liquid phase transitions that varied based on the nature of the sample. The melting points of complexes 1-6 was also determined by melting point apparatus. In addition, we observed the decomposition point of the LMONs materials, which presumably underwent oxidation reactions with air.

Complex **2** exhibited a melting point of 134.73°C with a range of 8 °C (Fig 3.1). An oxidation induction time experiment on complex **2** shown in (Fig 3.5) revealed that the material undergoes stepwise decomposition at three exothermic points: T1=232.07°C, T2=291.07°C and T3=429.07°C.

Complex **3** exhibited a melting point of 134.73°C with a range of 8°C (Fig 3.2). An oxidation induction time on Complex **3** (Fig 3.6), revealed that the material undergoes stepwise decomposition at two exothermic points: T1= 267.40°C and T2= 421.07°C.

Complex **4** exhibited a melting point of 135.74 °C with a range of 9°C (Fig 3.3). An oxidation induction time on complex **4** (Fig 3.7), revealed that the material undergoes stepwise decomposition at two exothermic points: T1=269.07°C, T2=423.40°C.

Complex **5** exhibited a melting point of 122.4°C with a range of 20°C Fig (3.4). An oxidation induction time on complex **5** (Fig 3.8) revealed that the material undergoes stepwise decomposition at three exothermic points: T1=289.73°C T2=381.98°C, T3=393.07°C.

Complex **6** data is included in the appendix section.

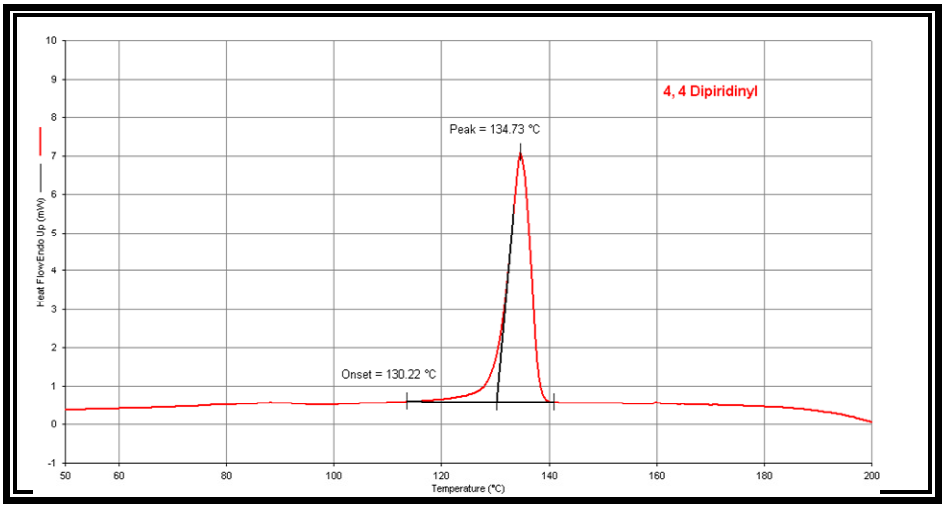

Figure 3.1: Melting point of complex 2 determined by DSC

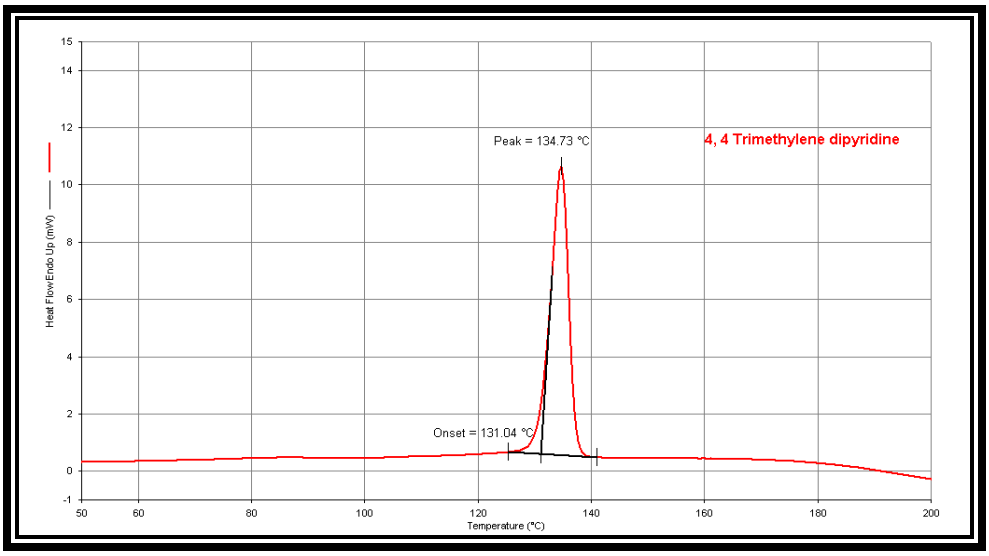

Figure 3.2: Melting point of complex 3 determined by DSC.

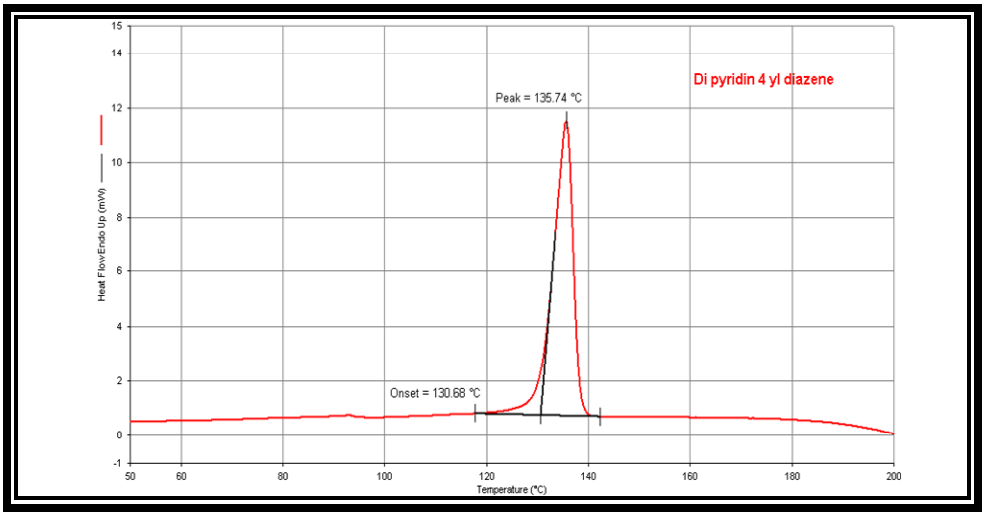

Figure 3.3: Melting point of complex 4 determined by DSC.

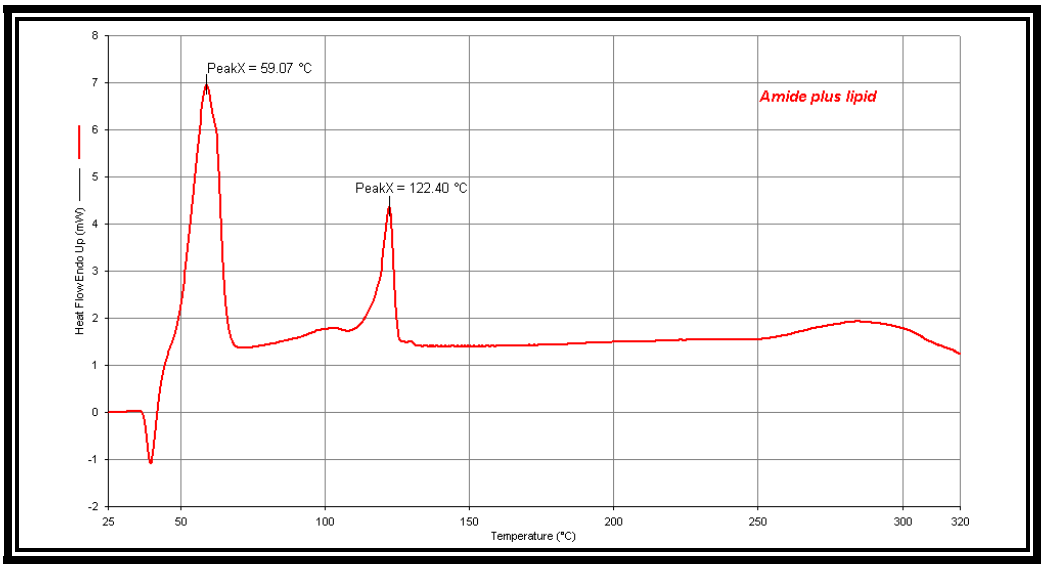

Figure 3.4: Melting point of Complex 5 determined by DSC.

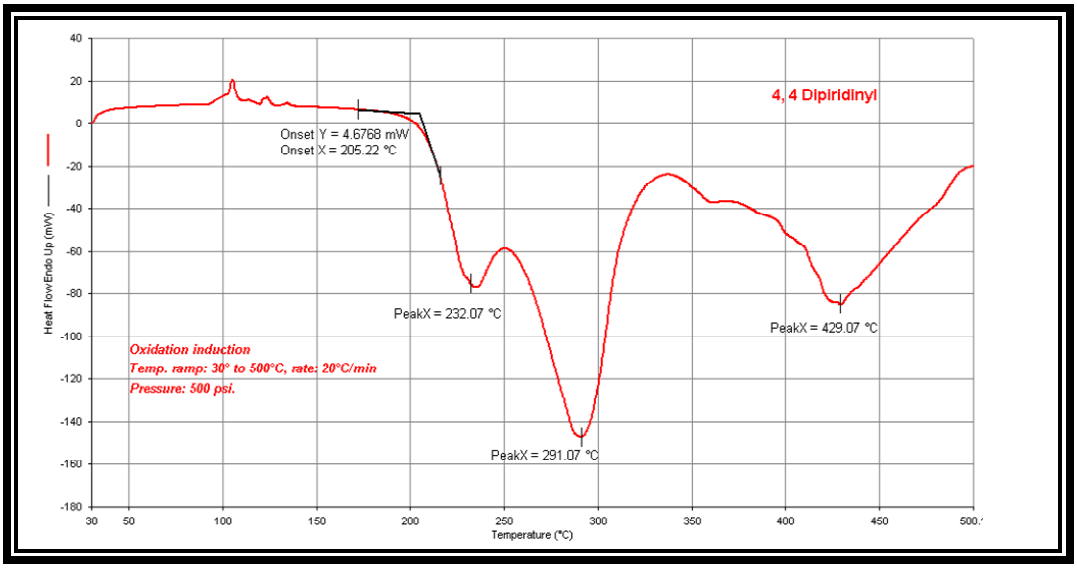

Figure 3.5: the graph illustrates oxidation induction time of complex 2.

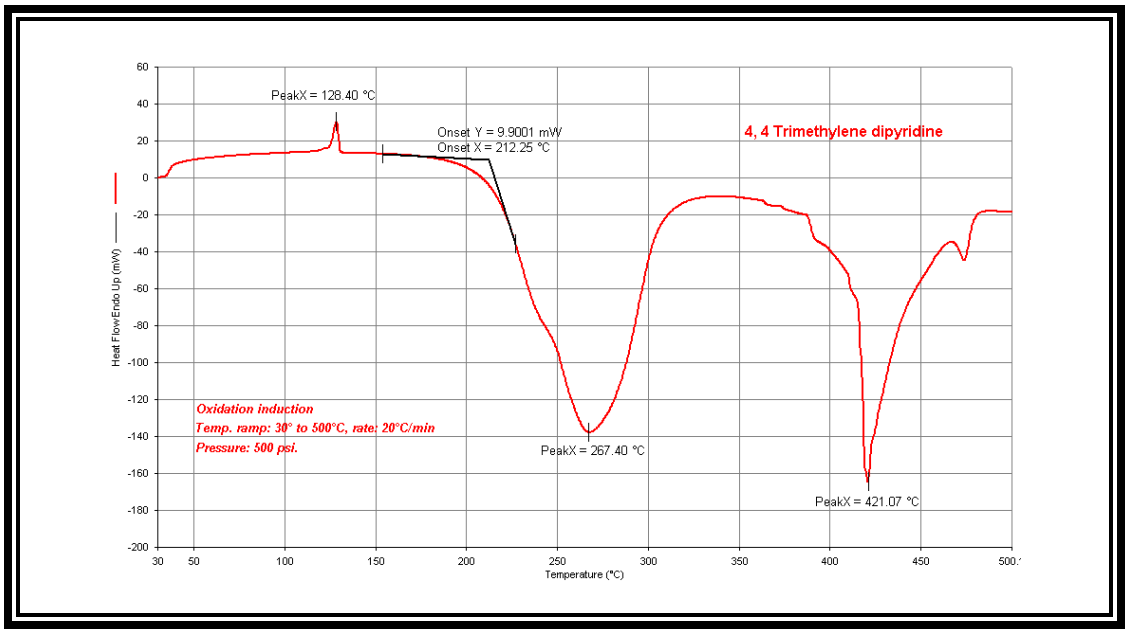

Figure 3.6: the graph illustrates Oxidation induction time of complex 3.

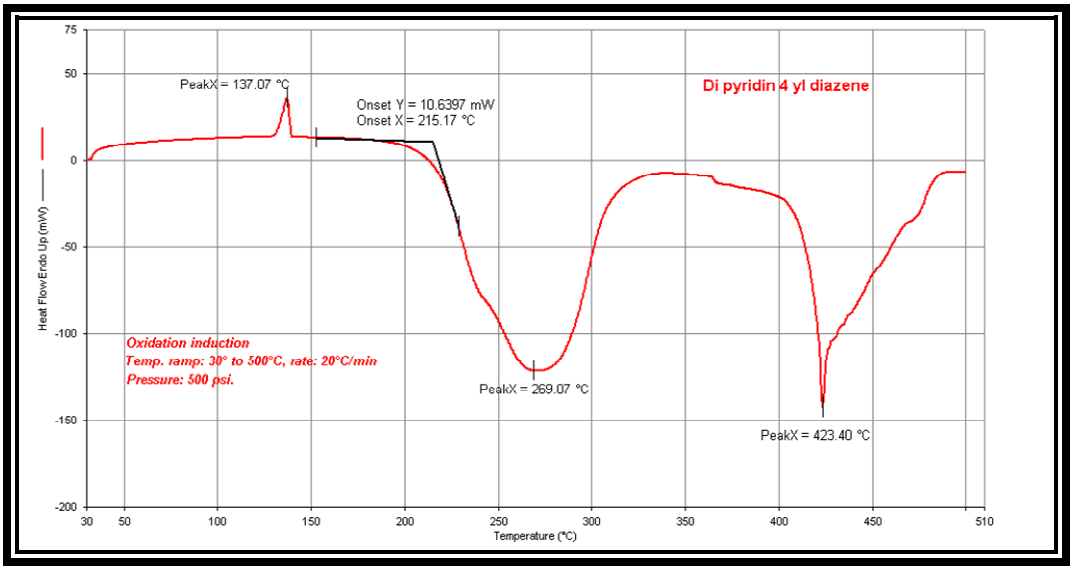

Figure 3.7: the graph illustrates oxidation induction time of complex 4.

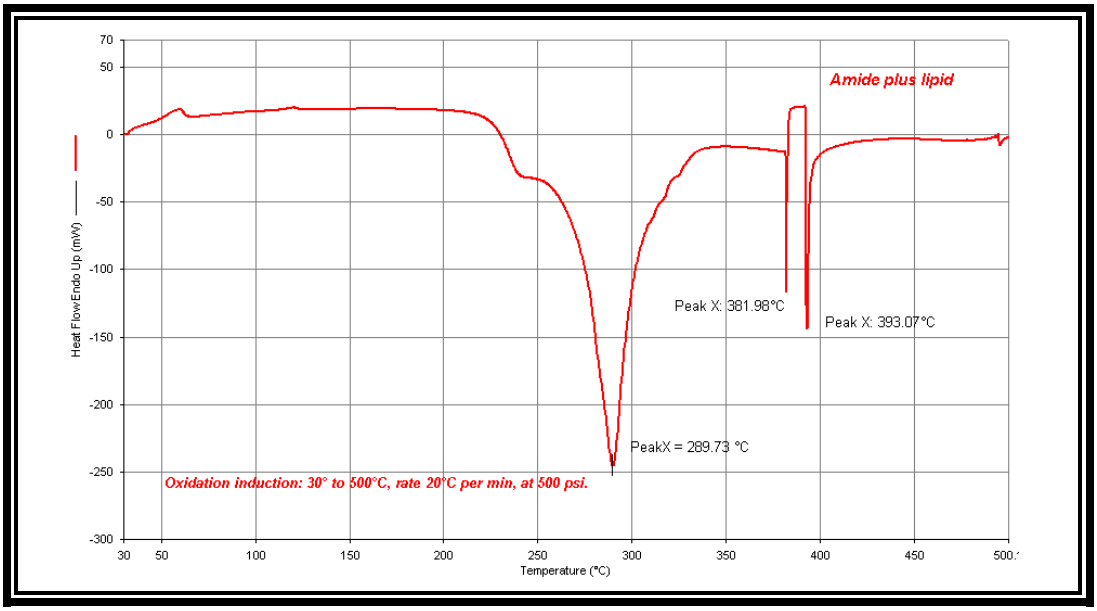

Figure 3.8: The graph illustrates oxidation induction time of Complex 5.

3.2 THERMO GRAVIMETRIC ANALYSIS (TGA)

Thermo gravimetric analysis (TGA) was used to determine the changes in weight and degradation temperatures by monitoring material stability and its fraction of volatile components. This approach provides the ash content and the oxidation temperature.

TGA curve of Zn-complex **2** exhibits three main steps of weight losses (Fig. 3.9). The first step started at 46.39 °C and completed at 347.42°C. This step is the weight lost of ligand. The weight lost of lipid ionic bonding starts at 350°C and finished at 556.75°C. Weight lost is 65% of the sample. The decomposition of the remaining phase starts at 556.75 °C.

TGA of curve of Zn-complex **3** exhibits three main steps of weight losses (Fig 3.10). The first step initiates at 46.63°C and completed at 364.82°C. This step is the weight lost of ligand. The weight lost of ligand initiate at 366.64°C and finished at 558.73°C loosing 64.95% of weight. Last step initiate at 558.73 °C and finished at 798.87°C.

TGA curve of Zn-complex **4** exhibits three main steps of weight losses (Fig. 3.11). The first step started at 46.40 °C and completed at 350.65°C. This step is the weight lost of ligand. The weight lost of lipid ionic bonding starts at 350°C and finished at 556.42 °C. Weight lost is 66% of the sample. The decomposition of the remaining phase starts at 556.42 and finished at 797.8°C.

TGA curve of Zn-complex **5** exhibits three main steps of weight losses (Fig. 3.12). The first step started at 45.23 °C and completed at 291.40°C. This step is the weight lost of ligand. The weight lost of lipid ionic bonding starts at 291°C and finished at 557.85 °C. Weight lost is 36% of the sample. The decomposition of the remaining phase starts at 557.85 and finished at 799.83°C

TGA curve data of Zn-complex **6** is included in the appendix section.

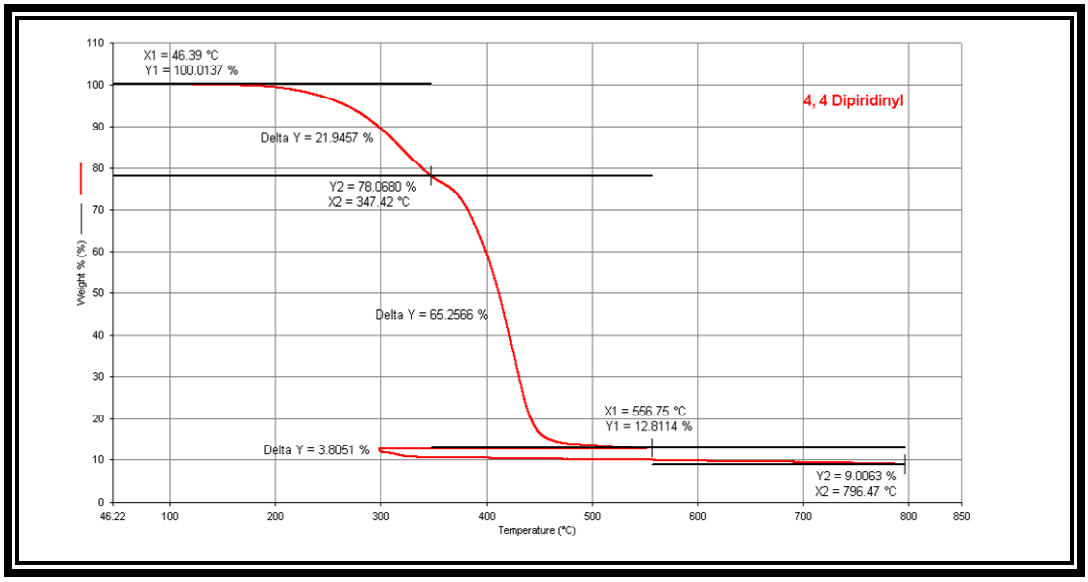

Figure 3.9: TGA curve of complex 2.

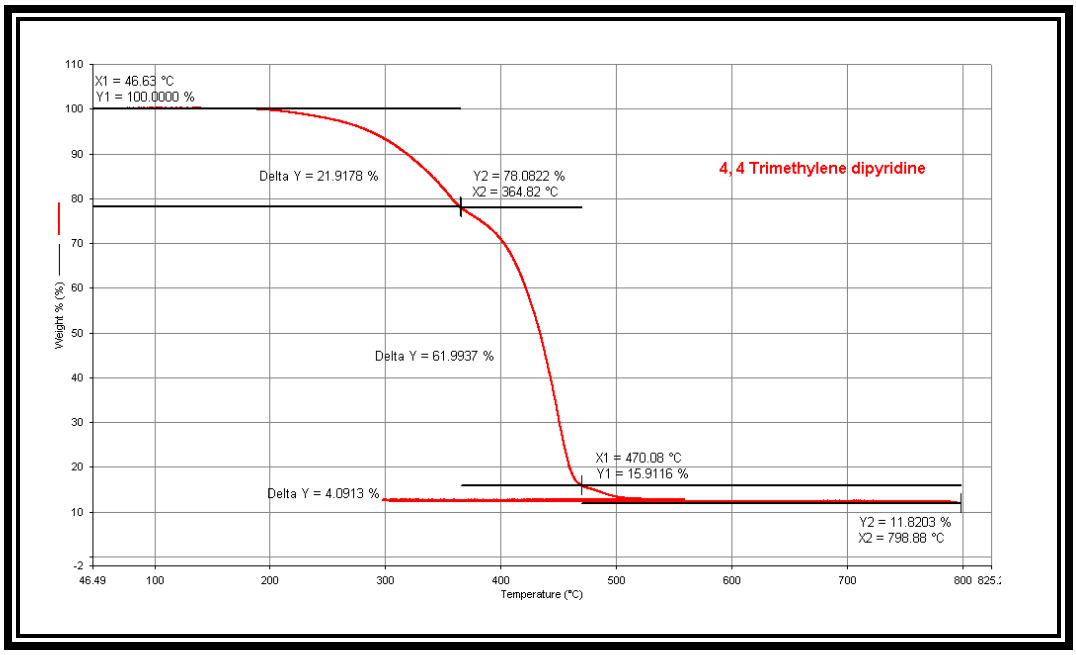

Figure 3.10: TGA curve of complex 3 .

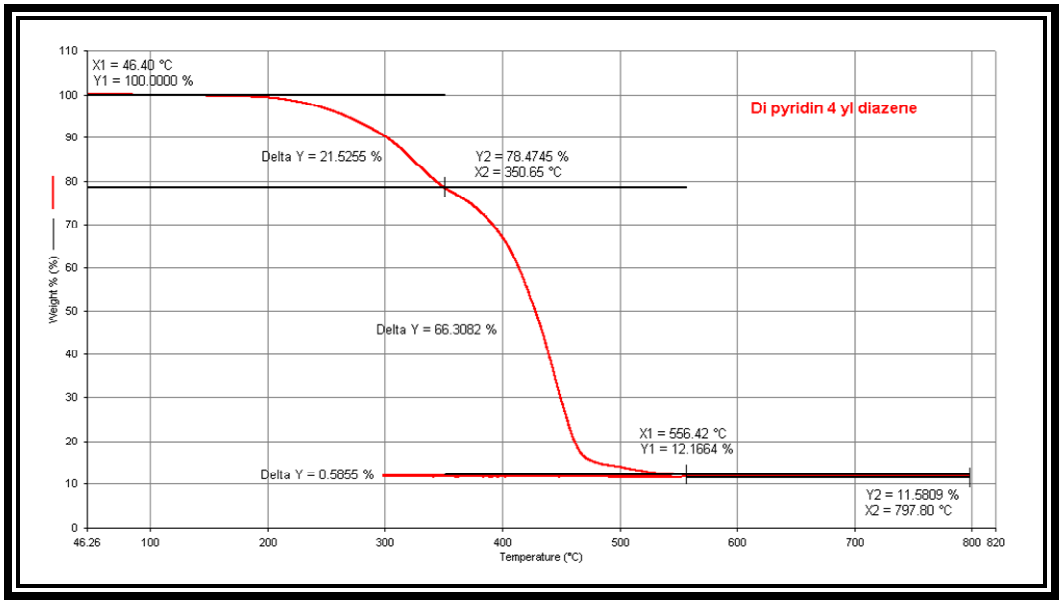

Figure 3.11: TGA curve of complex 4.

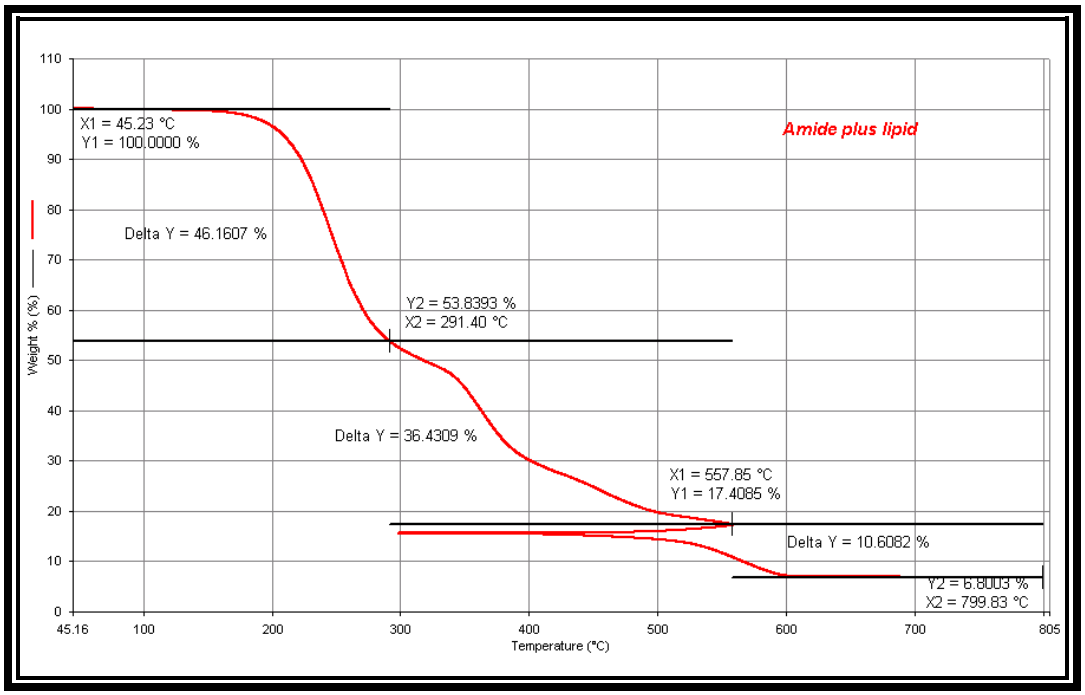

Figure 3.12: TGA curve of complex 5.

3.3 DYNAMIC LIGHT SCATTERING (DLS)

Dynamic light scattering (DLS) used to determine the molecular mass of the soluble components of the LMON polymers **2**-**5**. The LMON polymers were stirred in DMF until the solution was saturated. They were measured using the Precision Instruments DLS 1000 instrument, which is able to determine the average molecular mass of soluble polymers. The refraction index and viscosity of DMF was taken into consideration during the measurement.

The molecular mass of Zn-complex **2** was $4.14x10^2$ KDa (Figure 3.13). Zn-Complex **3** was $6.13x10^1$ KDa (Figure 3.14). Zn-complex **4** was $4.69x10^1$ KDa (Figure 3.15). Zn-complex **5** was $8.21x10^0$ KDa. (Figure. 3.16) and Zn-complex **6** before and after UV was $1.33x10^1$KDa (Figure A.2.x) and $6.27x10^1$KDa (Figure A.2.x) respectively. Table 3.1 summarized the results shown below.

Table 3.1: Shows the Average molecular mass of LMONs.

Complex #	Molecular mass (KDa)
2	$4.14x10^2$
3	$6.13x10^1$
4	$4.69x10^1$
5	$8.21x10^0$
6 before UV	$1.33x10^1$
6 after UV	$6.27x10^1$

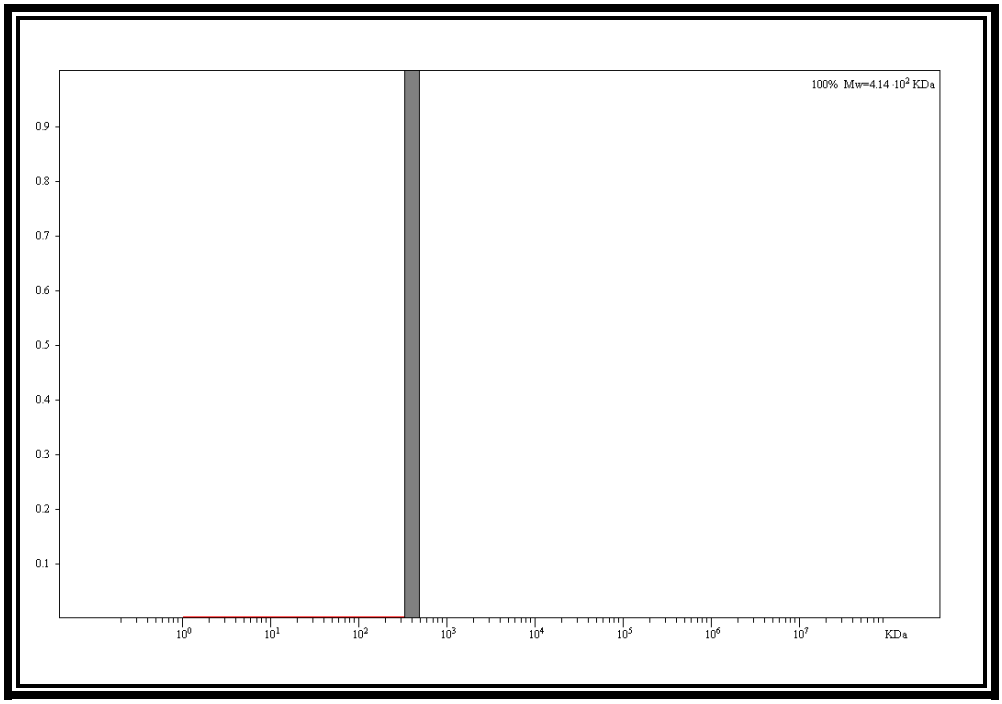

Figure 3.13: DLS of complex 2.

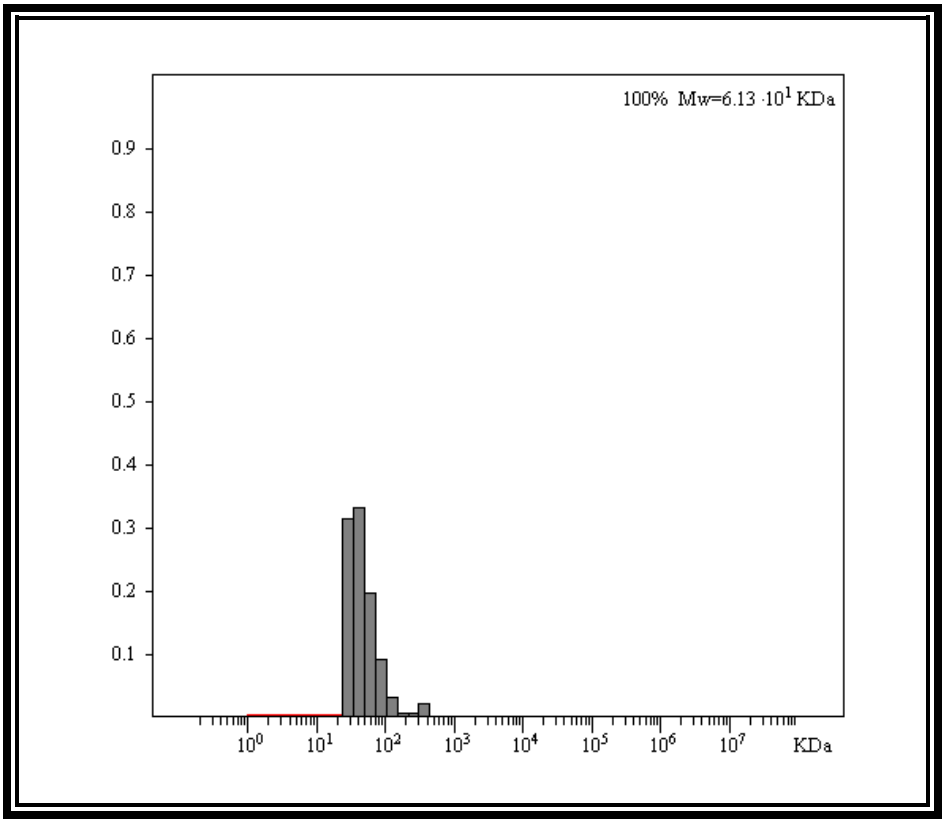

Figure 3.14: DLS of complex 3.

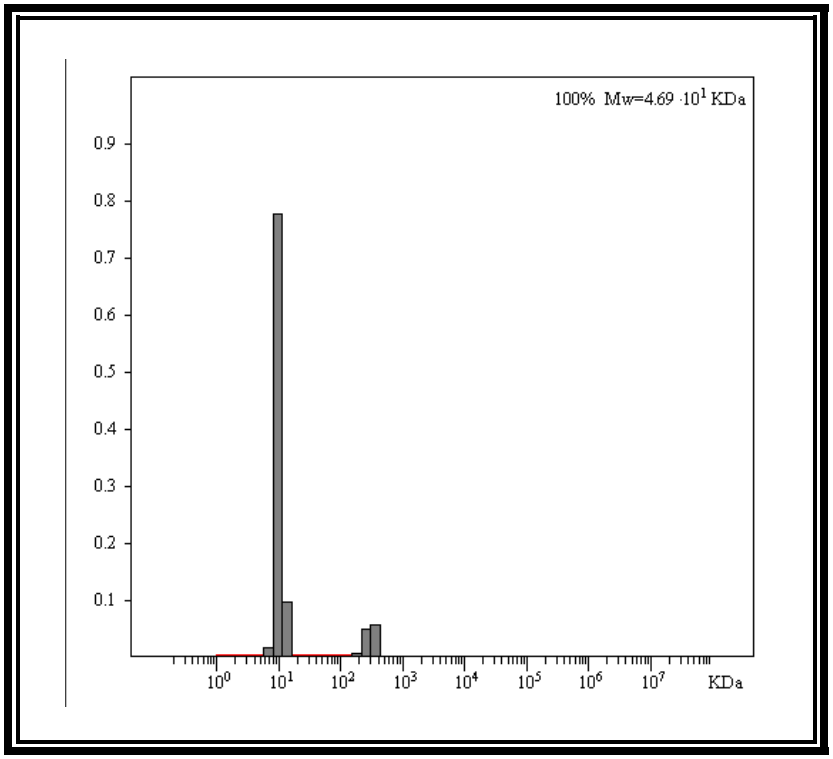

Figure 3.15: DLS of complex 4.

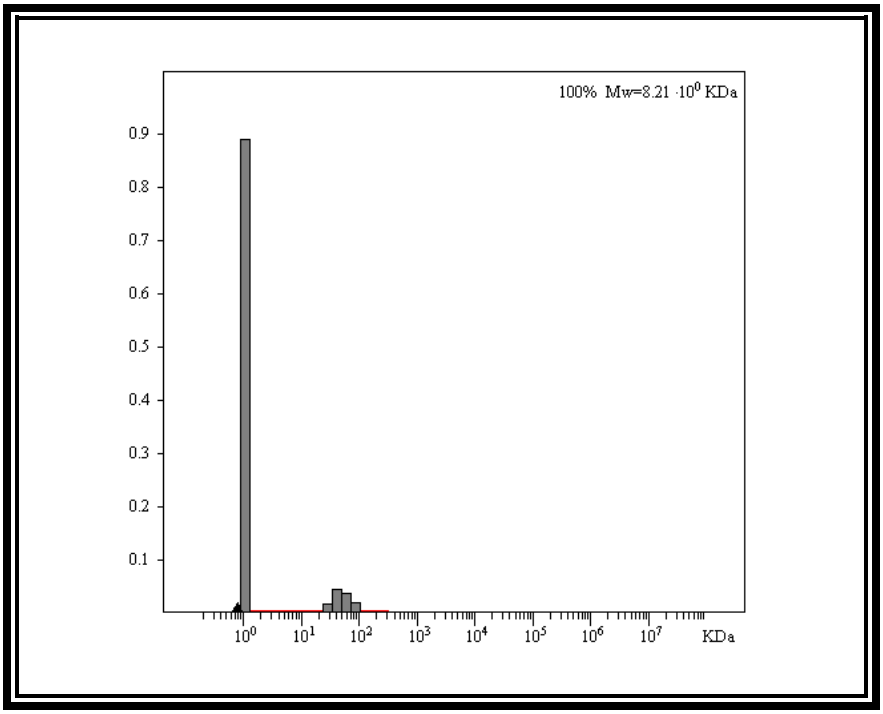

Figure 3.16: DLS of complex 5.

3.4 SELF- ASSEMBLY PROPERTIES

The LMON coordination polymers exhibit self-assembly properties according to optical polarized microscopy and X-ray powder diffraction. In particular, upon cooling from the isotropic melt state, the Zn-complex **2** forms a nematic phase that is clearly visible with optical polarized microscopy, Figure 3.17.

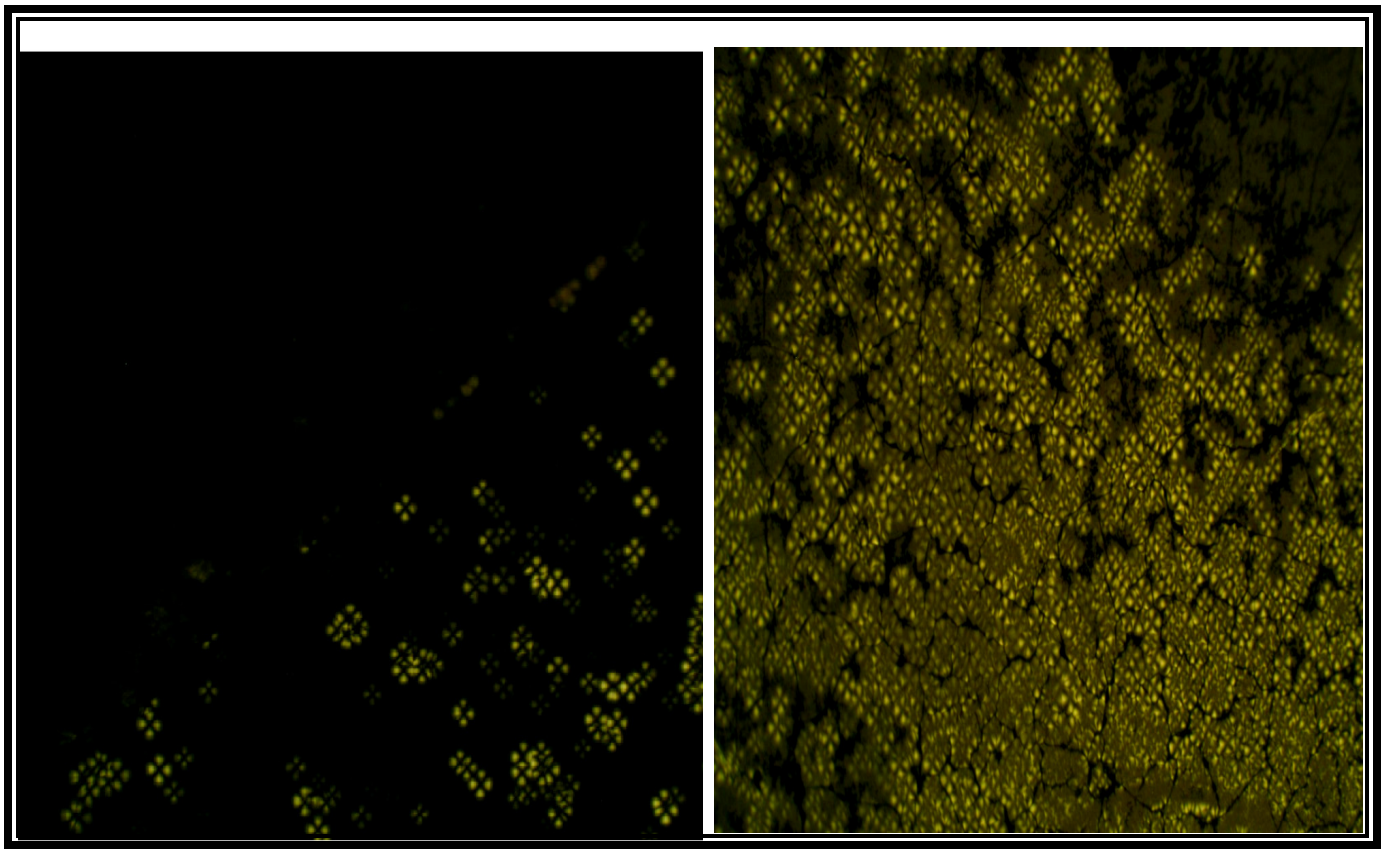

Figure 3.17: Optical polarized microscopy.

X-ray powder diffraction analysis of this phase indicates that a molecular order reminiscent of a microcrystalline material is evident, Figure 3.18.

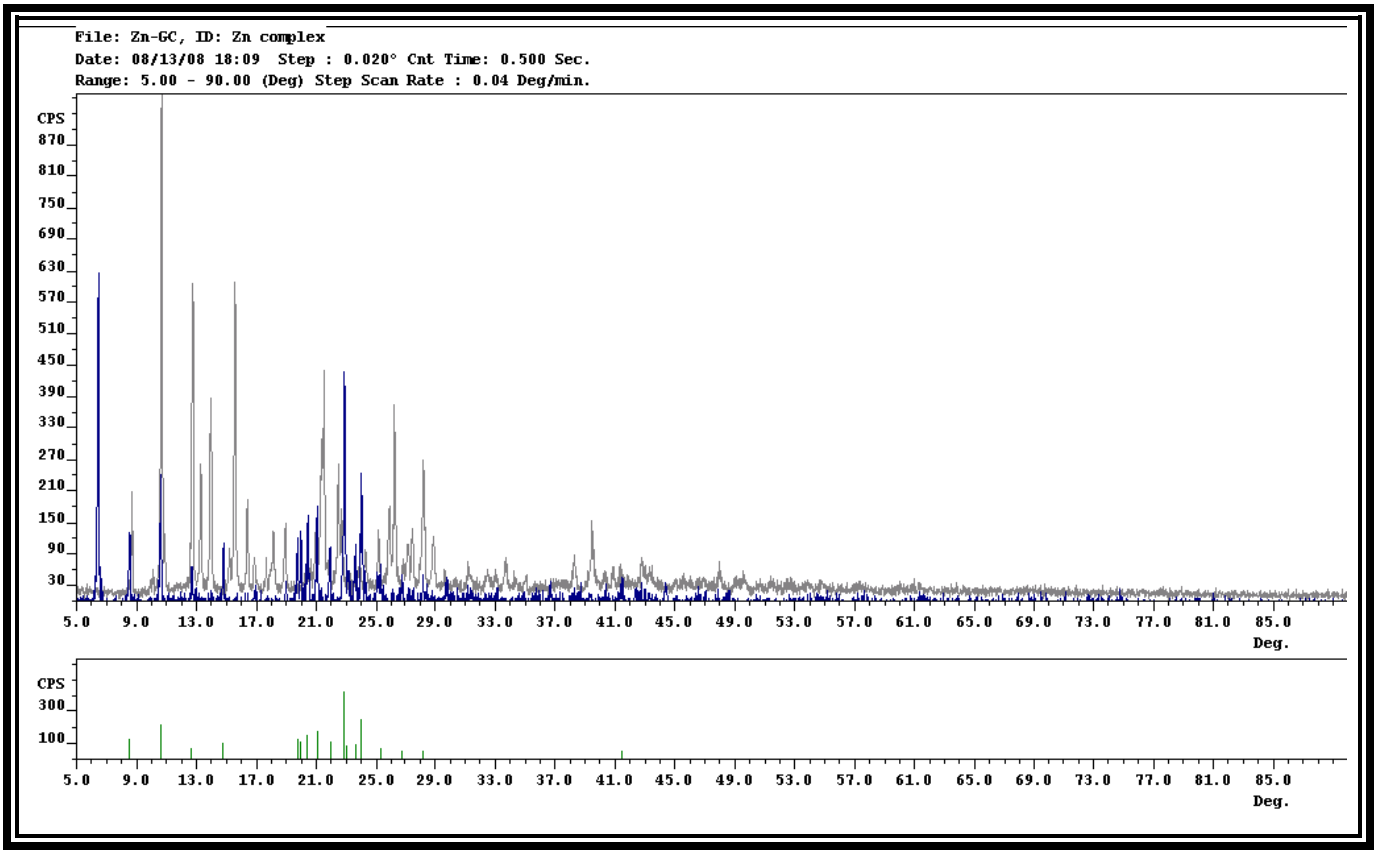

Figure 3.18: XRPD of Zn complex 2. Blue line describes Zinc (II) metal organic polymer, gray line describes melted Zinc (II) Metal Organic Polymer.

SEM analysis of this phase also corroborated the crystallinity of the sample at this stage, Figure 3.19.

Figure 3.19: SEM image of Zn complex 2.

3.5 POST-ASSEMBLY MODIFICATIONS

The Zn-complex 6 derived from purely biomass crudes (raw canola oil extracts) contains 86% unsaturated hydrocarbon chains. Canola oil has the most uniformity in terms of degrees of saturation. We predicted that the fact that canola oil has 85%+ olefins, the products may be photoactive and upon UV exposure, these groups may crosslink. Therefore, we performed an experiment in which the Zn-complex 6 was exposed to an intense source of UV (nm) for 18 h, a change in the physical properties was observed. For example, the melting point changed by 8 °C small change in the melting point indicates a chemical change presumably the cross linking of the olefins, Figure 3.20. Infrared analysis also indicates that after photo activation the double bond which appears in the functional region C=C 3006 wave number, (Figure 3.21) before UV is reduced to single bond C-C as is shown in (Figure 3.22) after UV.

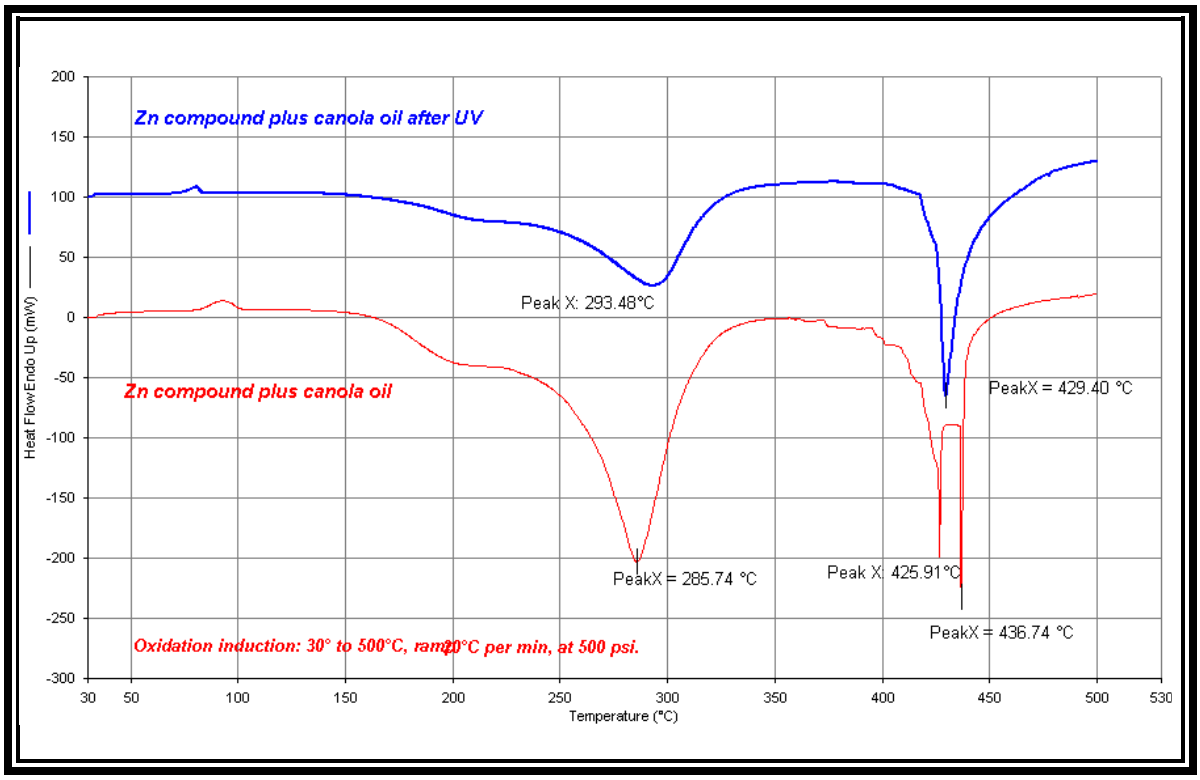

Figure 3.20: The melting point of Zn complex 6 exhibits a small change indicating cross linking of the olefins.

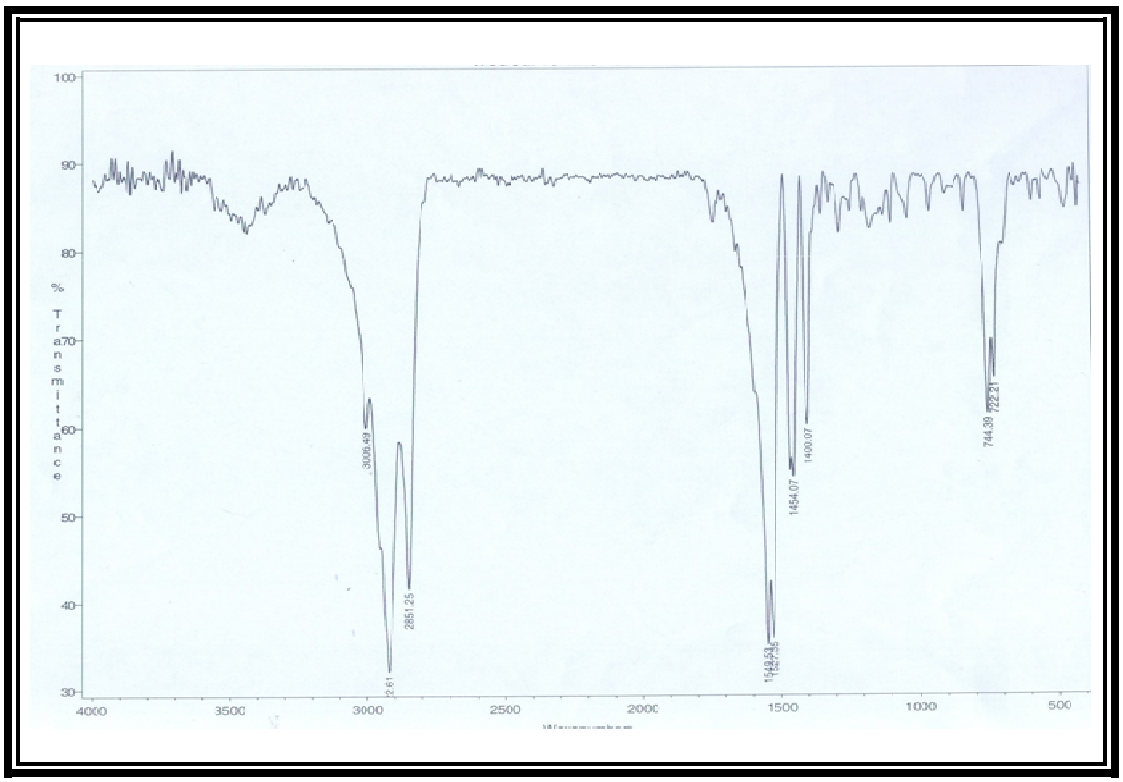

Figure 3.21: IR of Zn-Complex 6 before UV exposure.

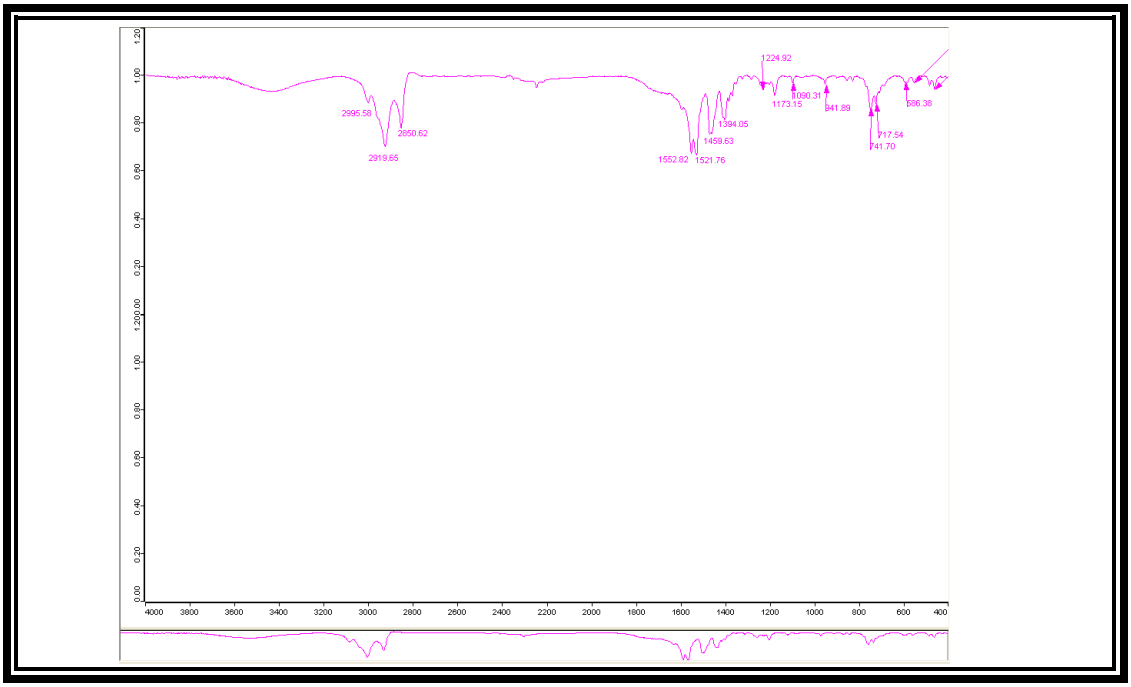

Figure 3.22: IR of Zn-Complex 6 after UV exposure.

Conclusions

In this thesis the synthesis and characterization of LMON coordination polymers was presented. Complex **1** provided the atomic structure of the metal organic network. Zn-Complex **2** to **5** provide the first examples of LMONs coordination polymers and Zn-complex **6** was the first LMON coordination polymer with fatty acid components derived directly form biomass.

In addition, we reported that a chemical change can be observed in Zn-complex **6** after being exposed to UV-radiation due to cross linking of the olefin in the unsaturated fatty acids. It can be concluded that after photo-activation the unsaturated fatty acids components of LMONs are reduced to a single bond due to cross linking process in the sample. Future work will involve analysis of the electrical and mechanical properties and other physical properties of these new materials.

References

1. James, S.L. Chem Soc. Rev. 2003, 32, 276-288.

2.De Lill Daniel T. Templated Metal-Organic Frameworks. Candidacy Examination Ph. D. http://www.clicktoconvert.com]

3. Janiak, C.J. Chem. Soc., Dalton Trans. 2003, 2781-2804.

4. (a) Nouar, F.; Eubank, J.F.; Bousquet, T.; Wojtas, L.; Zaworotko, M.J.;Eddaoudi, M.J.Am Chem Soc. 2008, 130, 1833-1835.

(b) Chen, B.; Ockwing, N. W.; Millard, a. R.; Contreras, D. S.; Yaghi, O.M. Agnew. Chem. Int. Ed. 2005, 44, 4745-4749.

5. (a) Lee, E. Y.; Jang, S.Y.; Suh, M. P. J. Am. Chem. Soc. 2005, 127, 6374-6381.

(b) Dinca, M.; Long, J. R. J. Am. Chem. Soc. 2005 127, 9376-9377.

6. (a) Cho, S.-H.; Ma, B. –Q.; Nguyen, S.T,; Hupp, J.T. ; Albrecht-Schmitt, T.E. Chem. Commun. 2006, 2563-2565.

7. Shi, Z.;Li, G.; Wang, L.; Gao, L.; Chen, X.; Hua, J.; Feng, S. Cryst. Growth Des. 2004,4, 25-27.

8. Moeller, Therald., A Modern Introduction Inorganic Chemistry, John Wiley and Sons: New York,1982, 359.

9. Zumdahl, Steven S. Chemical Principles, Fifth Edition. New York: Houghton Miflin, 2005.943-946, 957.

10. Cotton, F.A. and Wilkinson, G., Advanced Inorganic Chemistry, John Wiley and Sons: New York, 1988 ISBN 97080471199575.

11. Cotton, F. A. "The Crystal Field Theory." Chemical Applications of Group Theory, 3rd ed. New York: Wiley, pp. 282-287, 1990.

12. Cotton, F. A.; Wilkinson, G.; and Gaus, P. Ch. 23 in Basic Inorganic Chemistry, 3rd ed. New York: Wiley, 1995.

13. Huheey, J. E.; Keiter, E. A.; and Keiter, R. L. Inorganic Chemistry: Principles of Structure and Reactivity, 4th ed. Reading, MA: Addison-Wesley, 1993

14. T. Yildrim and M.R. Hartman; Phys. Rev. Lett., 95, 215504 (2005); doi: 10.1103. Direct Observation of hydrogen adsorption sites and nano-cage formation in metal-organic frameworks (MOF).

15. NIST site: Direct Observation of Hydrogen adsorption Sites and Nano-Cage Formation in Metal-Organic Frameworks (MOF)

16. Metal-organic Frameworks with Exceptionally High Capacity for Storage of Carbon Dioxide at room temperature; Adrew R. Millward and Omar M. Yaghi; J. Am.Chem.Soc.; 2005; DOI: 10.1021/ja0570032.

17. California Air Resources Board. Motor Fuels Technical Review Chevron http://www.arb.ca.gov/html/homepage.htm]

18. Word Wide Fuel Charter, Technical Background. September 2006. Technical Background for Harmonised Fuel Recommendations Gasoline. Pages (17-19).]

19. Eddaoudi, Mohamed. Moler, David B. Li, Hailian. Chen, Banglin. Reineke, Theresa M. O'Keeffe, Michael. Yaghi, Omar M.2001. Accounts of Chemical Research, Volume 34, 319-330. Modular Chemistry: Secondary Building Units as a Basis for the Design of Highly Porous and Robust Metal-Organic Carboxylate Frameworks.

20. Modular Chemistry; Michl, J., Ed.; Kluwer Academic Publishers: Dordrecht, 1995, and references therein.

21. Bowes, C. L.; Ozin, G. A. Self-Assembling Frameworks: Beyond Microporous Oxides. Adv. Mater. 1996, 8, 13-28.

22. Cheetham, A. K.; Fe´rey, G.; Loiseau, T. Open-Framework Inorganic Materials. Angew. Chem., Int. Ed. 1999, 28, 3268-3292.

23. Hagrman, P. J.; Hagrman, D.; Zubieta, J. Organic-Inorganic Hybrid Materials: From "Simple" Coordination Polymers to Organodiamine-Templated Molybdenum Oxides. Angew. Chem.,Int. Ed. 1999, 38, 2638-2684.

24. Stein, A.; Keller, S. W.; Mallouk, T. E. Turning Down the Heat: Design and Mechanism in Solid-State Synthesis. Science 1993,259, 1558-1564.

25. Yaghi, O. M.; Li, H.; Davis, C.; Richardson, D.; Groy, T. L. Synthetic Strategies, Structure Patterns, and Emerging Properties in the Chemistry of Modular Porous Solids. Acc. Chem. Res. 1998, 31,474-484.

26. Hennigar, T. L.; MacQuarrie, D. C.; Losier, P.; Rogers, R. D.;Zaworotko, M. J. Supramolecular Isomerism in Coordination Polymers: Conformational Freedom of Ligands in [Co(NO3)2(1,2-bis(4-pyridyl)ethane)1.5]n. Angew. Chem., Int. Ed. Engl. 1997, 36, 972-973.

27. Batten, S. R.; Robson, R. Interpenetrating Nets: Ordered, Periodic Entanglement. Angew. Chem., Int. Ed. 1998, 37, 1460-1494.

28. Kitagawa, S.; Kondo, M. Functional Micropore Chemistry of Crystalline Metal Complex-Assembled Compounds. Bull. Chem. Soc. Jpn. 1998, 71, 1739-1753.

29. Blake, A. J.; Champness, N. R.; Hubberstey, P.; Li, W.-S.; Withersby,M. A.; Schro¨ der, M. Inorganic Crystal Engineering Using Self-Assembly of Tailored Building-Blocks. Coord. Chem. Rev.1999, 183, 117-138.

30. Lu, J.; Paliwala, T.; Lim, S. C.; Yu, C.; Niu, T.; Jacobson, A. J. Coordination Polymers of Co(NCS)2 with Pyrazine and 4,4¢-Bipyridine: Syntheses and Structures. Inorg. Chem. 1997, 36, 923-929.

31. Biradha, K.; Hongo, Yoshito, H.; Fujita, M. Open Square-Grid Coordination Polymers of the Dimensions 20 _ 20 Å: Remarkably Stable and Crystalline Solids Even after Guest Removal Angew.Chem., Int. Ed. 2000, 39, 3843-3845.

32. Xiong, R.-G.; Wilson, S. R.; Lin, W. Bis(Isonicotinato)Iron(II): A Rare, Neutral Three-Dimensional Iron Coordination Polymer. J.Chem. Soc., Dalton Commun. 1998, 4089-4090.

33. Chen, L.; Eddaoudi, M.; Hyde, S. T.; O'Keeffe, M.; Yaghi, O. M. Interwoven Metal-Organic Framework on a Periodic Minimal Surface with Extra-Large Pores. Science 2001, 291, 1021-1023.

34. Kepert, C. J.; Rosseinsky, M. J. Zeolite-Like Crystal Structure of an Empty Microporous Molecular Framework. Chem. Commun.1999, 375-376.

35. Goodgame, D. M. L.; Grachvogel, D. A.; Williams, D. J. A New Type of Metal-Organic Large-Pore Zeotype. Angew. Chem., Int.Ed. 1999, 38, 153-156.

36. Carlucci, L.; Ciani, G.; Proserpio, D. M. Interpenetrated and Noninterpenetrated Three-Dimensional Networks in the Polymeric Species Ag(tta) and 2 Ag(tta)âAgNO3(tta)tetrazolate): The First Examples of the *í*4-*è*1:*è*1:*è*1:*è*1 Bonding Mode for Tetrazolate. Angew. Chem., Int. Ed. 1999, 38, 3488-3492.

37. Kiang, Y.-H.; Gardner, G. B.; Lee, S.; Xu, Z.; Lobkovsky, E. B. Variable Pore Size, Variable Chemical Functionality, and an Example of Reactivity within Porous Phenylacetylene Silver Salts.J. Am. Chem. Soc. 1999, 121, 8204-8215.

38. Evans, Owen R. Lin, Wenbin. 2002. Accounts of Chemical Research, Volume 35, 511-522. Crystal Engineering of NLO Material Based on Metal Organic Coordination Networks.

39. Kim, Jaheon. Eddaoudi, Mohamed. Moler, David B. Li, Hailian. Chen, Banglin. Reineke, Theresa M. O'Keeffe, Michael. Yaghi, Omar M. 2001 Journal of American Chemical Society. Volume 123, 8239-8247. Assembly of Metal-Organic Frameworks from Large Organic and Inorganic Secondary Building Units: New Examples and Simplifying Principles for Complex Structures.

40. L. Pavia, Donald. M.Lapman, Gary. S.Kriz, George Jr. Ch 3 Introduction to spectroscopy: Sounders College Publishing. Philadelphia 1979.

41. Andrei, N. Khlobystov. Alexander,J. Blake. Neil R. Champness. Dmitrii A. Lemenovskii. Alexandre G. Majouga. NikolaiV. Zyk. Martin Schroder.2001 Coordination Chemistry Reviews, volume 222, 155-192. Supremolecular design of one-dimensional coordination polymers based on silve(I) complexes of aromatic nitrogen- donor ligands.

42. (a) K.A. Hirsch, S.R. Wilson, J.S. Moore, Chem Eur. J. 3 (1997) 765;

(b) A.J. Blake, N.R. Champness, P.A. Cooke, J.E.B. Nicolson, C. Wilson, J. Chem Soc. Dalton Trans. (2000) 3811.

Glossary

MOF= Metal Organic Framework

DN= Diamondoid Network

BTB= Benzene tribenzoate

BTC= Benzene tricarboxylate

Triflate= Trifluoromethane sulfonate

DMF= Dimethyl Formamide

DEF= Diethyl Formamide

TGA= Thermo Gravimetric Analysis

DSC= Differential Scanning Calorimeter

DLS= Dynamic Light Scattering

XRPD= X-Ray Powder Diffraction

FTIR= Fourier Transform Infrared Spectroscopy

SEM= Scanning Electron Microscopy

Appendix

A.1 SUPPORTING INFORMATION FOR CHAPTER 2.

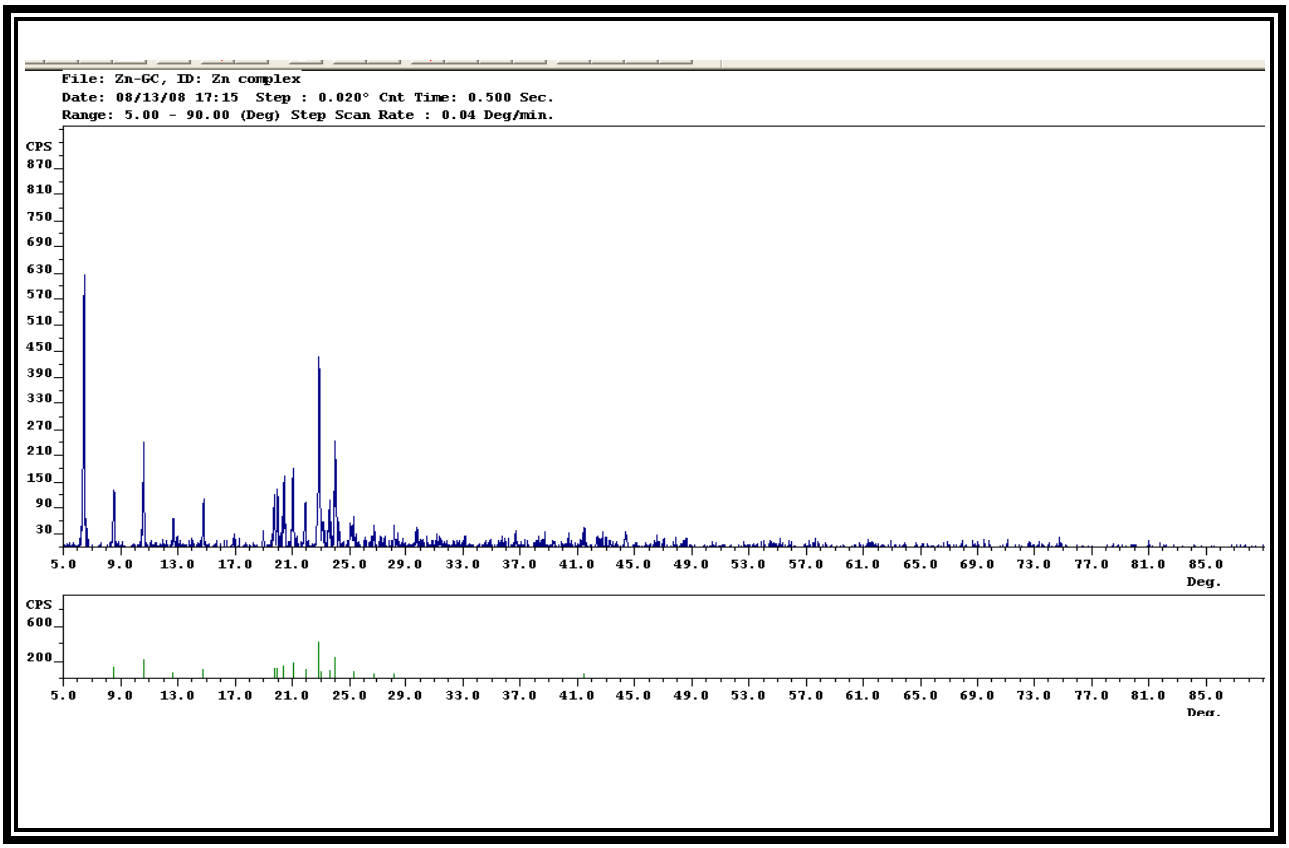

Figure A.1: XRPD of complex 1.

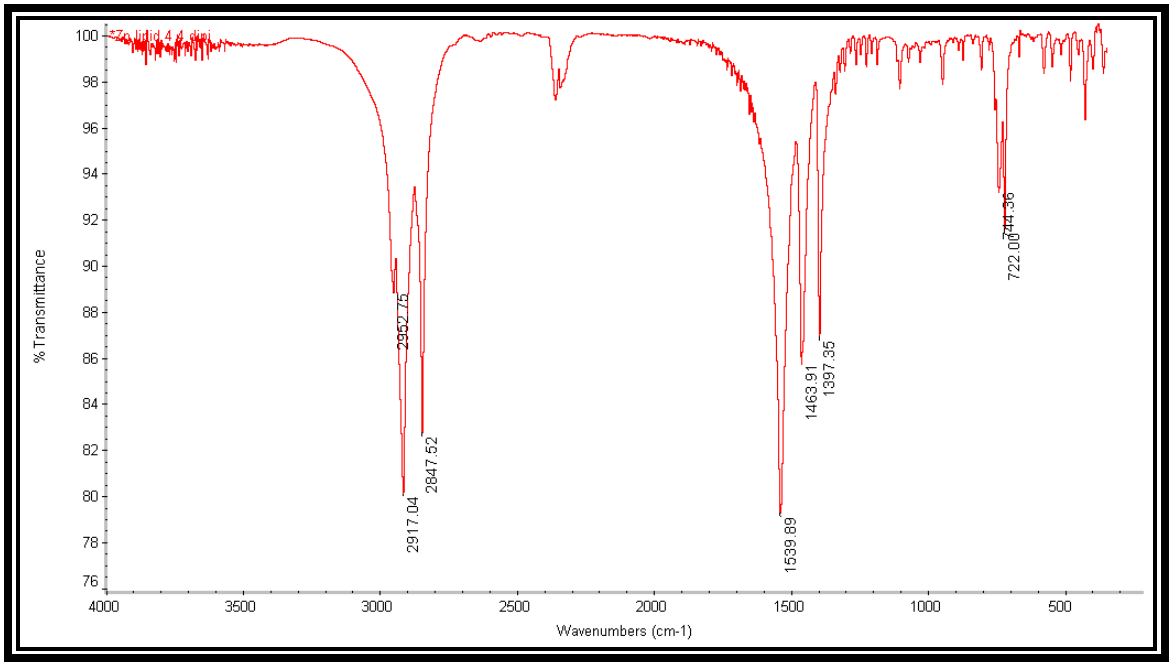

Figure A.2: FTIR of complex 2.

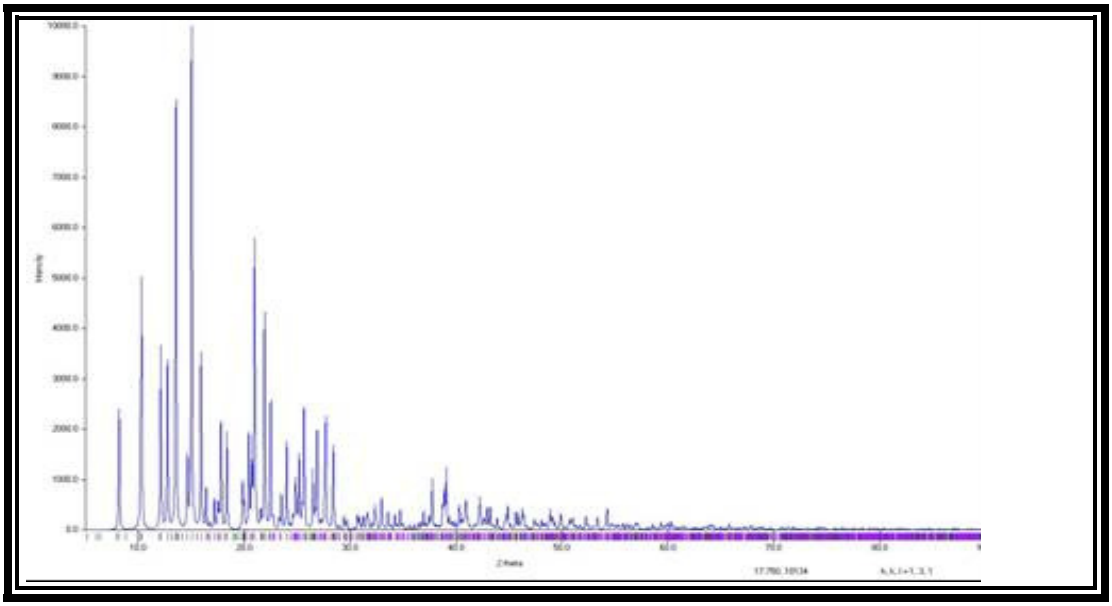

Figure A.3: Theoretical X-Ray powder diffraction from Zn crystals using 4,4'Trymethylene dipyridine (complex 3).

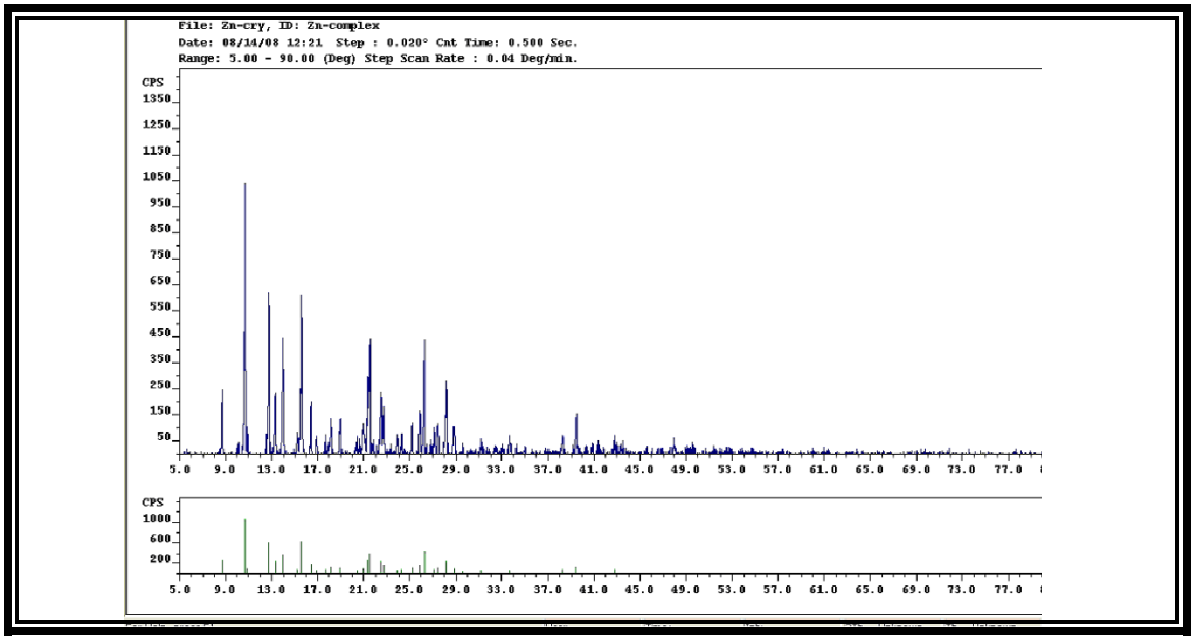

Figure A.4: Experimental X-Ray diffraction of complex 3.

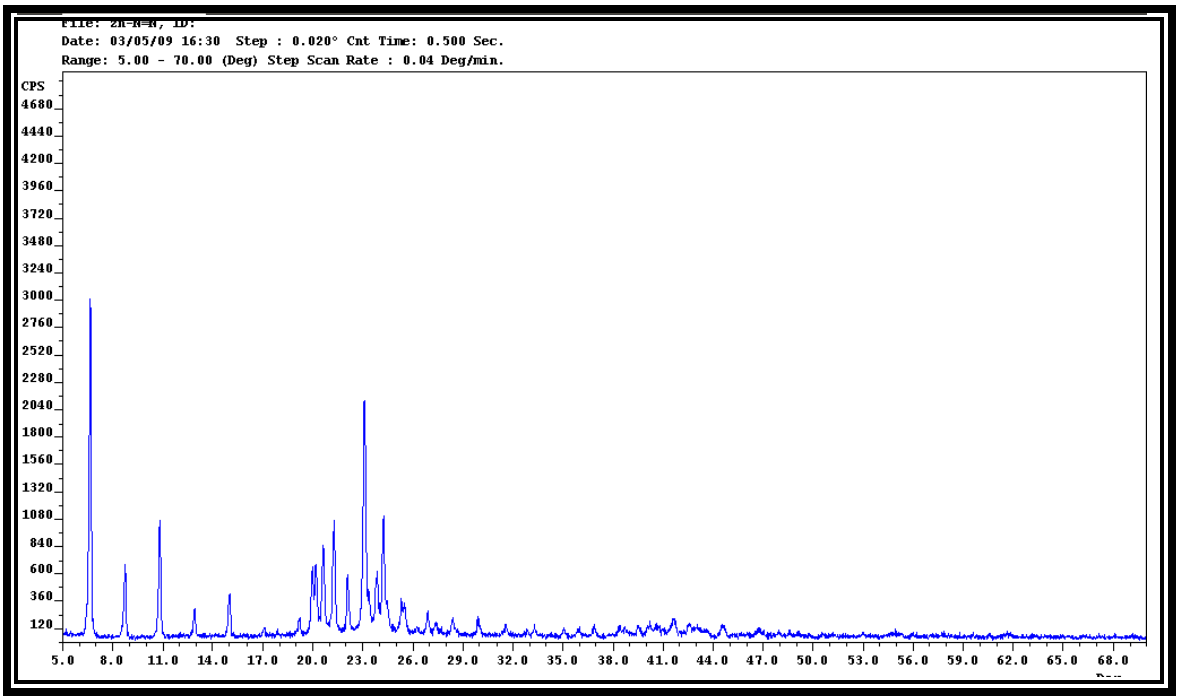

Figure A.5: XRPD of complex 4.

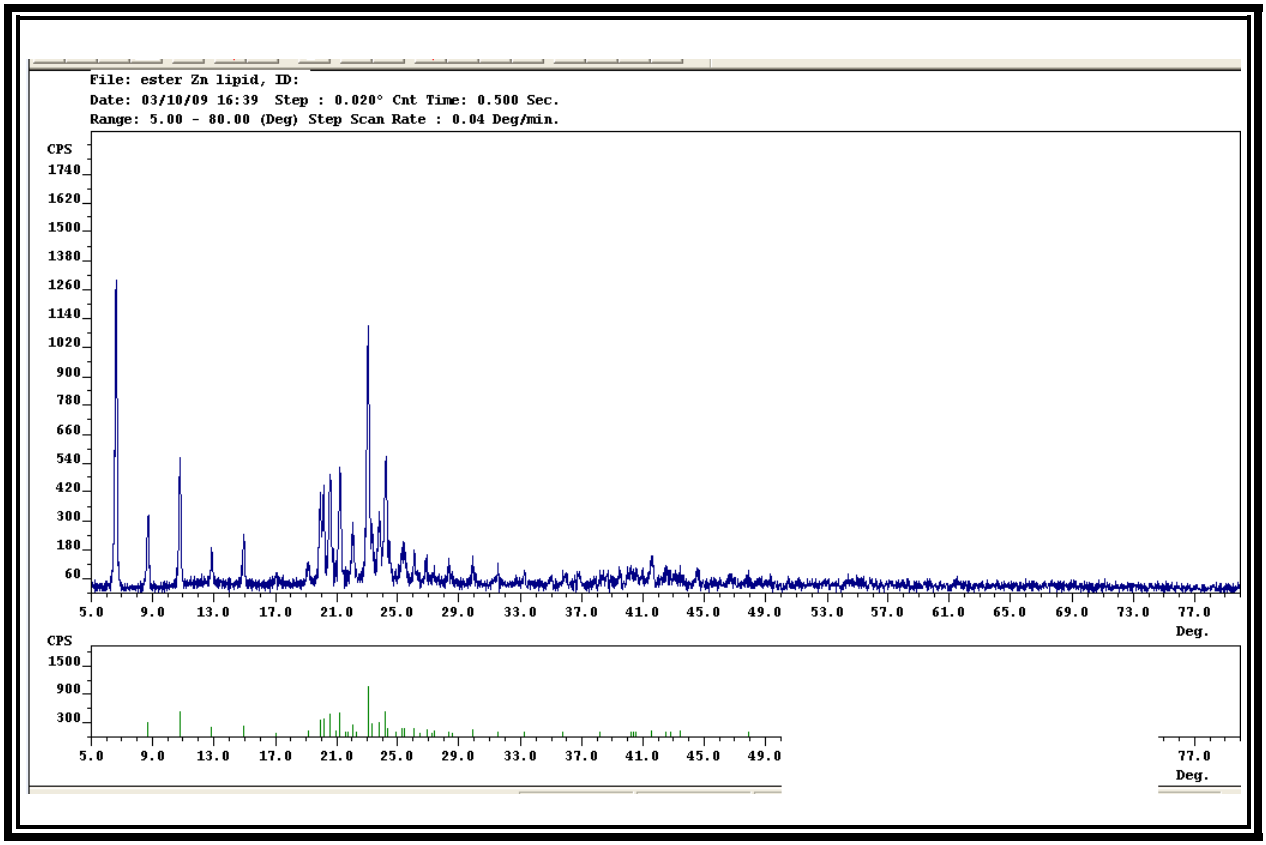

Figure A.6: XRDP of complex 5.

A.2 SUPPORTING INFORMATION FOR CHAPTER 3.

The derivative of (complex 6) was synthesized by reacting Zinc Trifluoromethane Sulfonate 5g, 4, 4'-Trymethylene dipyridine 2.73g and canola oil 7.76 g dissolved in 30 ml of DMF. The reaction was left in reflux approximately 48 hours. The molecular weight of repetitive unit was 826.56. The calculated percentage by mass was C=71.2034%, H=9.7551%, N=3.3892%, O=7.7424%, and Zn=7.9111%, and the yield percentage was 24.02%. The reaction is illustrated in figure A.2.1.

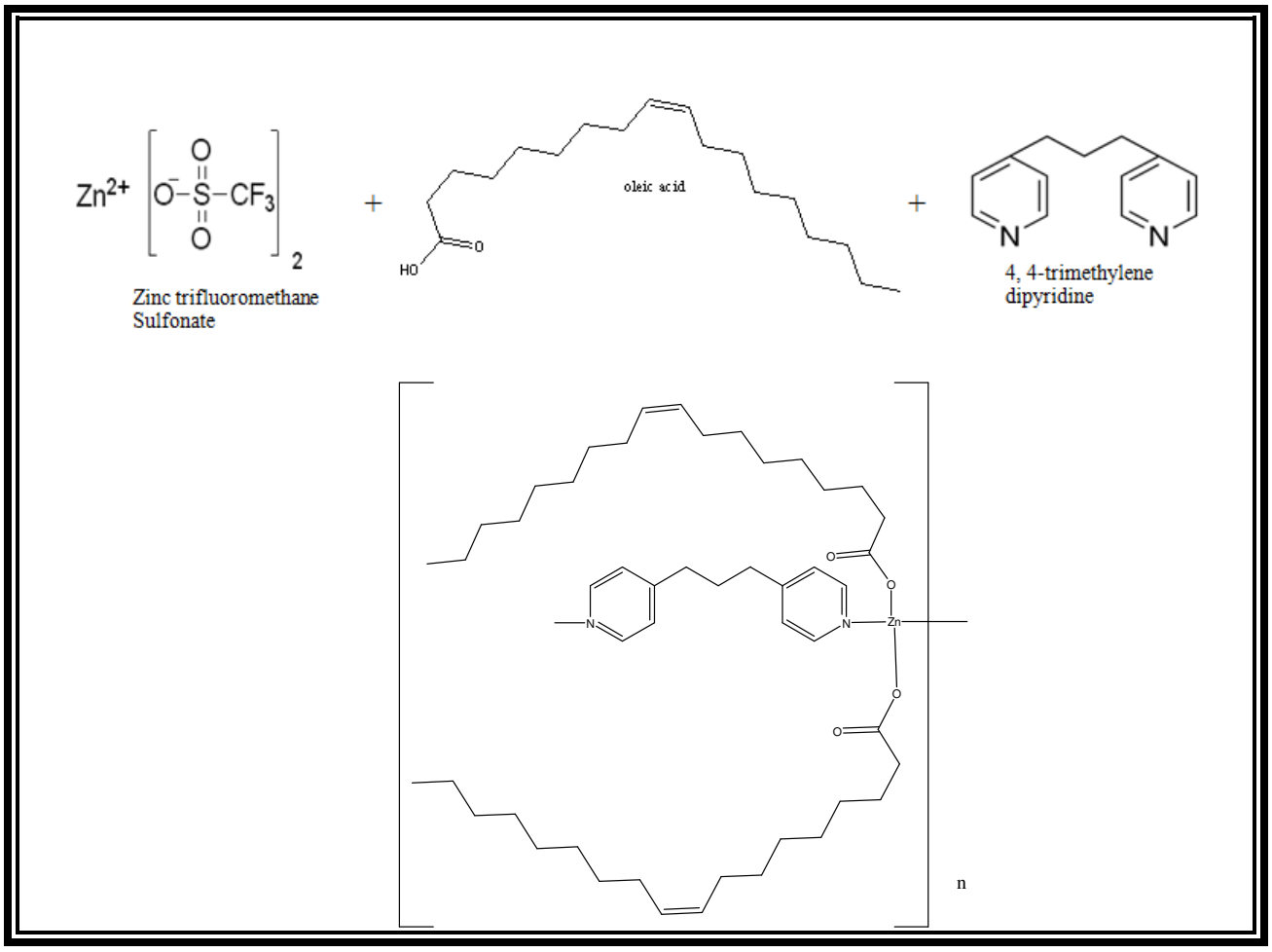

Figure A.2.1: Synthesis of Zn-complex 6.

A.2.1 DIFFERENTIAL SCANNING CALORIMETER (DSC)

Complex 6 exhibited a melting point of 92.07°C with a range of 8 °C (Fig A.2.2). An oxidation induction time experiment on complex **6** shown in (Fig 2.2.3), revealed that the material undergoes stepwise decomposition at three exothermic points: T1=285.74°C, T2=425.91 and T3=436.74°C.

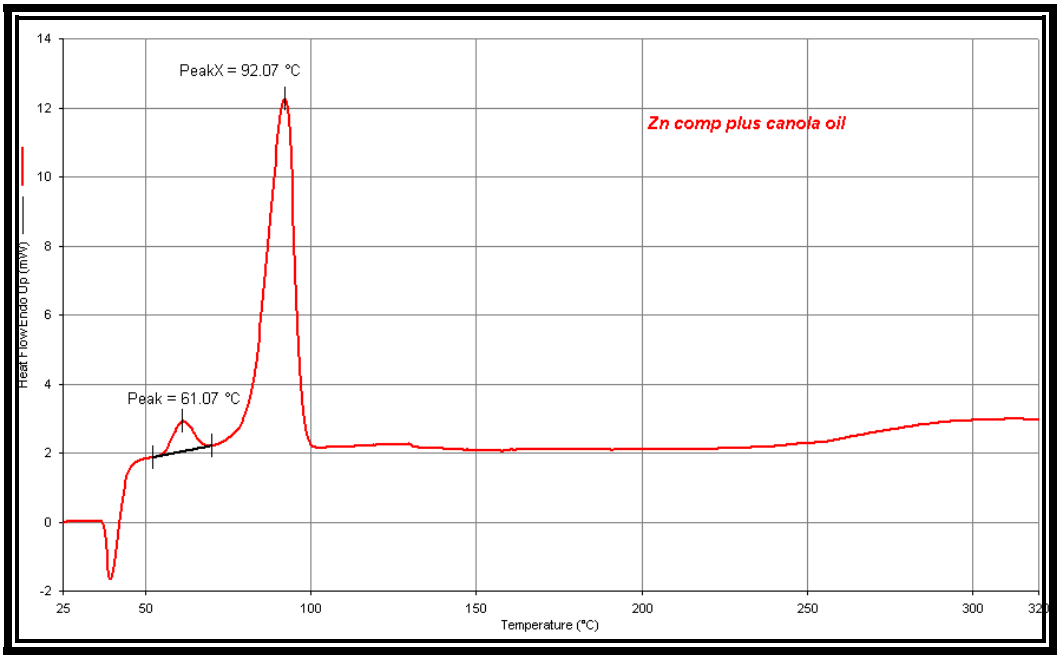

Figure A.2.2: Melting point of Zn-complex 6.

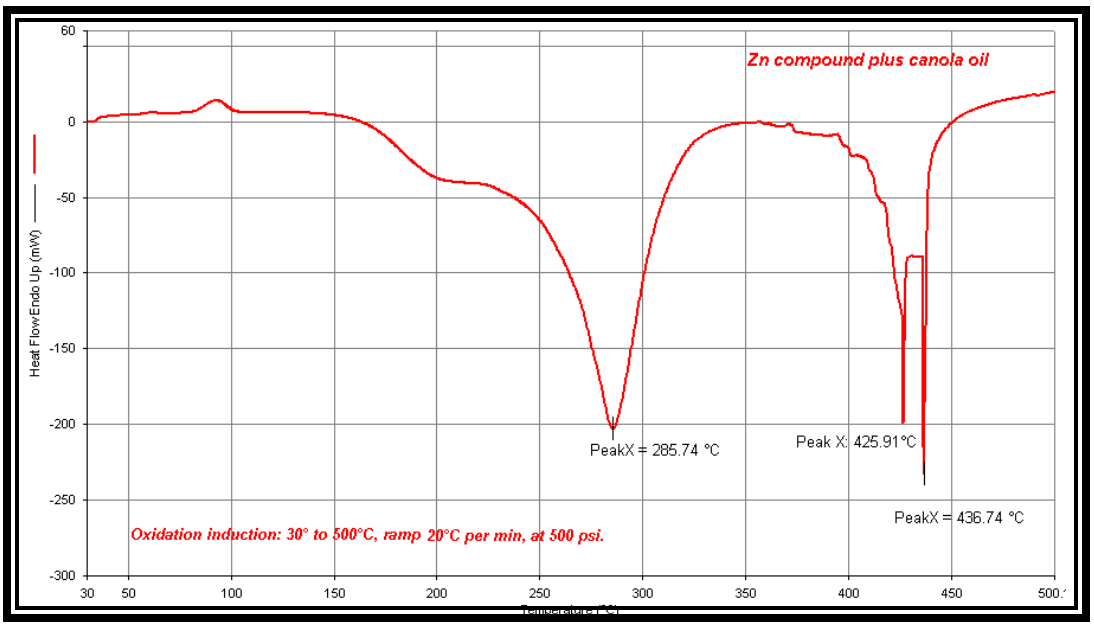

Figure A.2.3: Oxidation induction time of Zn-complex 6.

Complex 6 was mixed with azobisonitrile photoactive and then exposed to UV 18 hrs. The oxidation induction time shown in (Figure A.2.4), revealed a phase change after photo activation at two exothermic points: T1=293.48°C and T2=429.40°C.

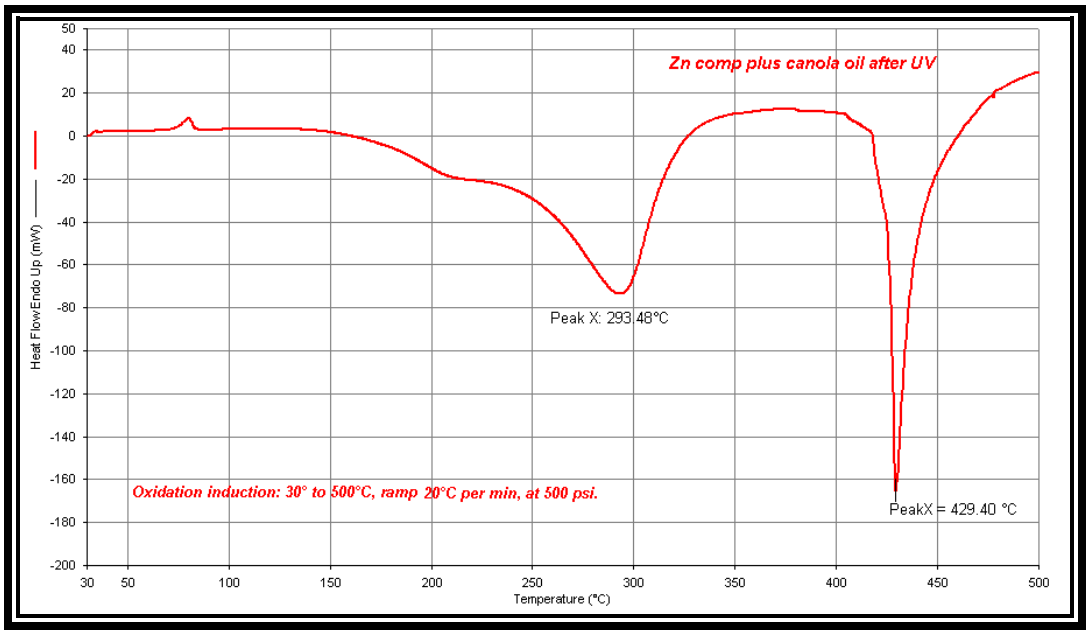

Figure A.2.4: Oxidation induction time of complex 6 after UV exposure.

A.2.2 THERMO GRAVIMETRIC ANALYSIS (TGA)

TGA curve of Zn-complex **6** exhibits three main steps of weight losses (Fig. A.2.5). The first step started at 45.22 °C and completed at 348.25°C. This step is the weight lost of ligand. The weight lost of lipid ionic bonding starts at 348.25°C and finished at 469.56 °C. Weight lost is 60% of the sample. The decomposition of the remaining phase starts at 469.56 and finished at 799.82°C

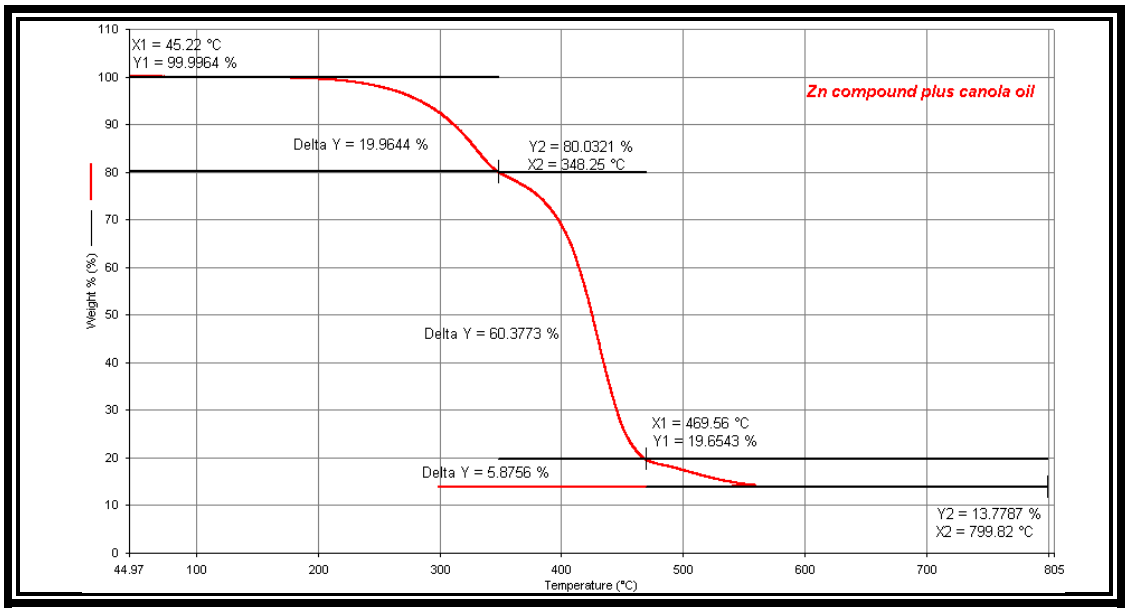

Figure A.2.5: TGA of Complex 6.

Curriculum Vita

Maria Eugenia Martinez Ortega was born in Chihuahua, Chihuahua. The only daughter of Maria Luisa Ortega and Enrique Martinez, she graduated from Universidad Autónoma de Chihuahua, Chihuahua, Chihuahua, with bachelor degree in Engineering Chemistry. She worked full time in Delphi Automotive from 1997 until present. In the fall of 2003 she entered the Graduate School at the University of Texas at El Paso to pursue her Master's degree in Chemistry. A poster of this work was presented during the Conference of American Chemical Society. Salt Lake City, Utah 2009.

Permanent address: Berea Norte #615
Ciudad Juárez, Chihuahua, 32540

This thesis/dissertation was typed by Maria Eugenia Martinez Ortega.